

Weakly supervised causal representation learning

Johann Brehmer*
Qualcomm AI Research[†]
jbrehmer@qti.qualcomm.com

Pim de Haan*
Qualcomm AI Research[†]
QUVA Lab, University of Amsterdam
pim@qti.qualcomm.com

Phillip Lippe
QUVA Lab, University of Amsterdam
p.lippe@uva.nl

Taco Cohen
Qualcomm AI Research[†]
tacos@qti.qualcomm.com

Abstract

Learning high-level causal representations together with a causal model from unstructured low-level data such as pixels is impossible from observational data alone. We prove under mild assumptions that this representation is however identifiable in a weakly supervised setting. This involves a dataset with paired samples before and after random, unknown interventions, but no further labels. We then introduce implicit latent causal models, variational autoencoders that represent causal variables and causal structure without having to optimize an explicit discrete graph structure. On simple image data, including a novel dataset of simulated robotic manipulation, we demonstrate that such models can reliably identify the causal structure and disentangle causal variables.

1 Introduction

The dynamics of many systems can be described in terms of some high-level variables and causal relations between them. Often, these causal variables are not known but only observed in some unstructured, low-level representation, such as the pixels of a camera feed. Learning the causal representations together with the causal structure between them is a challenging problem and may be important for instance for applications in robotics and autonomous driving [1]. Without prior assumptions on the data-generating process or supervision, it is impossible to uniquely identify the causal variables and their causal structure [2, 3].

In this work, we show that a weak form of supervision is sufficient to identify both the causal representations and the structural causal model between them. We consider a setting in which we have access to data pairs, representing the system before and after a randomly chosen, unknown intervention while preserving the noise. This may approximate the generative process of data collected from a video feed of an external agent or demonstrator interacting with a system. Neither labels on the intervention targets nor active control of the interventions are

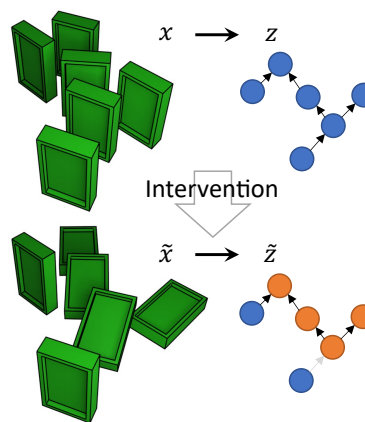


Figure 1: We learn to represent pixels x as causal variables z . The bottom shows the effect of intervening on one variable. We prove that variables and causal model can be identified from samples (x, \tilde{x}) .

*Equal contribution

[†]Qualcomm AI Research is an initiative of Qualcomm Technologies, Inc.

necessary for our identifiability theorem, making this setting useful for offline learning. We prove that with this form of weak supervision, and under certain assumptions (including that the interventions are stochastic and perfect and that all interventions occur in the dataset), latent causal models (LCMs)—structural causal models (SCMs) together with a decoder from the causal factors to the data space—are identifiable up to a relabelling and elementwise reparameterizations of the causal variables.

We then discuss two practical methods for LCM inference. First, we define explicit latent causal models (ELCMs) as a variational autoencoder (VAE) [4] in which the causal variables are the latent variables and the prior is based on an SCM. While this approach works in simple problems, it can be finicky and is difficult to scale. We trace this to a major challenge in causal representation learning, namely that it is a chicken-and-egg problem: it can be difficult to learn the causal variables when the causal graph is not yet learned, and it is difficult to learn the graph without knowing the variables.

To overcome this optimization difficulty, we introduce a second model class: implicit latent causal models (ILCMs). These models can represent causal structure and variables *without* requiring an explicit, discrete graph representation, which makes gradient-based optimization easier. Nevertheless, these models still contain the causal structure implicitly, and we discuss two algorithms that can extract it after the model is trained. Finally, we demonstrate ILCMs on synthetic datasets, including the new CausalCircuit dataset of a robot arm interacting with a causally connected system of light switches. We show that these models can robustly learn the true causal variables and the causal structure from pixels.

2 Related work

Our work builds on the work of Locatello et al. [5] on *disentangled representation learning*. The authors introduce a similar weakly supervised setting where observations are collected before and after unknown interventions. In contrast to our work, however, they focus on disentangled representations, i. e. (conditionally) independent factors of variation with a trivial causal graph, which our work subsumes as a special case. Other relevant works on disentangled representation learning and (nonlinear) independent component analysis include Refs. [6–12].

The problem of *causal representation learning* has been gaining attention lately, see the recent review by Schölkopf et al. [1]. Lu et al. [13] learn causal representations by observing similar causal models in different environments. von Kügelgen et al. [14] use the weakly supervised setting to study self-supervised learning, using a known but non-trivial causal graph between content and style factors. Lippe et al. [15] learn causal representations from time-series data from labelled interventions, assuming that causal effects are not instantaneous but can be temporally resolved. Yang et al. [16] propose to train a VAE with an SCM prior, but require the true causal variables as labels. Other relevant works include Refs. [17–21]. To the best of our knowledge, our work is the first to provide identifiability guarantees for arbitrary, unknown causal graphs in this weakly supervised setting.

3 Identifiability of latent causal models from weak supervision

In this section, we show theoretically that causal variables and causal mechanisms are identifiable from weak supervision. In Sec. 4 we will then demonstrate how we can learn causal models in practice by training a causally structured VAE.

3.1 Setup

We begin by defining latent causal models and the weakly supervised setting. Here, we only provide informal definitions and assume familiarity with common concepts from causality as introduced for instance in Ref. [22]. We provide a complete and precise treatment in Appendix A.1 and discuss limitations of our setup and possible generalizations in Appendix B.

We describe the causal structure between latent variables as a Structural Causal Model (SCM). An SCM \mathcal{C} describes the relation between causal variables z_1, \dots, z_n with domains \mathcal{Z}_i and noise variables $\epsilon_1, \dots, \epsilon_n$ with domains \mathcal{E}_i along a directed acyclic graph (DAG) $\mathcal{G}(\mathcal{C})$. Causal mechanisms $f_i : \mathcal{E}_i \times \prod_{j \in \text{pa}_i} \mathcal{Z}_j \rightarrow \mathcal{Z}_i$ describe how the value of a causal variable is determined from the associated noise variables, as well as the values of its parents in the graph. Finally, an SCM includes a probability measure for the noise variables.

An SCM entails a unique solution $s : \mathcal{E} \rightarrow \mathcal{Z}$ defined by successively applying the causal mechanisms. We require the causal mechanisms to be pointwise diffeomorphic, that is, for any value of the parents z_{pa_i} , we have that $f_i(\cdot; z_{\text{pa}_i})$ is invertible, differentiable, and its inverse is differentiable.³ Then s is also diffeomorphic and thus noise variables can be uniquely inferred from causal variables. This simplifies the weakly supervised distribution, as the only stochasticity comes from the noise variables and the intervention. The SCM also entails an observational distribution $p_{\mathcal{C}}(z)$ (Markov with respect to the graph of the SCM), which is the pushforward of $p_{\mathcal{E}}$ through the solution.

A perfect, stochastic intervention $(I, (f_i)_{i \in I})$ modifies an SCM by replacing for a subset of the causal variables, called the intervention target set $I \subset \{1, \dots, n\}$, the causal mechanism f_i with a new mechanism $\tilde{f}_i : \mathcal{E}_i \rightarrow \mathcal{Z}_i$, which does not depend on the parents. The intervened SCM has a new solution $\tilde{s}_I : \mathcal{E} \rightarrow \mathcal{Z}$. We call interventions atomic if the number of targeted variables is one or zero.

We will reason about generative models in a data space \mathcal{X} , in which the causal structure is latent. Also including a distribution of interventions (as in Ref. [23]), we define LCMs:

Definition 1 (Latent causal model (LCM)). *A latent causal model $\mathcal{M} = \langle \mathcal{C}, \mathcal{X}, g, \mathcal{I}, p_{\mathcal{I}} \rangle$ consists of*

- an acyclic SCM \mathcal{C} , which is faithful (all independencies are encoded in its graph [24]),
- an observation space \mathcal{X} ,
- a decoder $g : \mathcal{Z} \rightarrow \mathcal{X}$ that is diffeomorphic onto its image,
- a set \mathcal{I} of interventions on \mathcal{C} , and
- a probability measure $p_{\mathcal{I}}$ over \mathcal{I} .

We define two LCMs as equivalent if all of their components are equal up to a permutation of the causal variables and elementwise diffeomorphic reparameterizations of each variable, see Fig. 2.

Definition 2 (LCM isomorphism (informal)). *Let $\mathcal{M} = \langle \mathcal{C}, \mathcal{X}, g, \mathcal{I}, p_{\mathcal{I}} \rangle$ and $\mathcal{M}' = \langle \mathcal{C}', \mathcal{X}, g', \mathcal{I}', p'_{\mathcal{I}'} \rangle$ be two LCMs with identical observation space. An LCM isomorphism between them is a graph isomorphism $\psi : \mathcal{G}(\mathcal{C}) \rightarrow \mathcal{G}(\mathcal{C}')$ together with elementwise diffeomorphisms for noise and causal variables that tell us how to reparameterize them, such that the structure functions, noise distributions, decoder, intervention set, and intervention distribution of \mathcal{M}' are compatible with the corresponding elements of \mathcal{M} reparameterized through the graph isomorphism and elementwise diffeomorphisms. \mathcal{M} and \mathcal{M}' are equivalent, $\mathcal{M} \sim \mathcal{M}'$, if and only if there is an LCM isomorphism between them.*

Following Locatello et al. [5], we define a generative process of pre- and post-interventional data:⁴

Definition 3 (Weakly supervised generative process). *Consider an LCM \mathcal{M} where the underlying SCM has continuous noise spaces \mathcal{E}_i , independent probabilities $p_{\mathcal{E}_i}$, and admits a solution s . We*

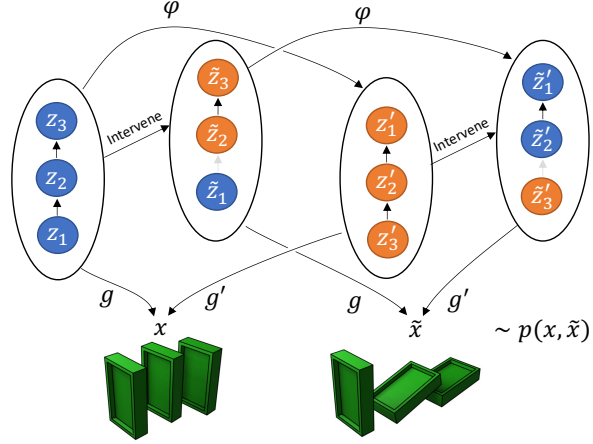


Figure 2: In LCM \mathcal{M} , z_i denotes whether the i -th stone from the front is standing. Intervening on the second variable, z_2 , leads to \tilde{z} . The decoder g renders z, \tilde{z} as images x, \tilde{x} . LCM \mathcal{M}' has an equivalent representation in which z'_i denotes whether the i -th stone from the back has fallen. In Thm. 1, we prove that if and only if two causal models have the same pixel distribution $p(x, \tilde{x})$, there exists an LCM isomorphism φ : an element-wise reparameterization of the causal variables plus a permutation of the ordering that commutes with interventions and causal mechanisms.

³Under some mild smoothness assumptions, any SCM can be brought into this form by elementwise redefinitions of the variables, preserving the observational and interventional distributions, but not the weakly supervised / counterfactual distribution.

⁴This construction is closely related to twinned SCMs [25, Def. 2.17], typically used to compute counterfactual queries $p(\tilde{z}_{\setminus I} | z, \tilde{z}_I)$. We instead focus on the joint distribution of pre-intervention and post-intervention data.

define the weakly supervised generative process of data pairs $(x, \tilde{x}) \sim p_{\mathcal{M}}^{\mathcal{X}}(x, \tilde{x})$ as follows:

$$\begin{aligned} \epsilon &\sim p_{\mathcal{E}}, & z &= s(\epsilon), & x &= g(z), \\ I &\sim p_{\mathcal{I}}, & \forall i \in I, \tilde{\epsilon}_i &\sim p_{\tilde{\mathcal{E}}_i}, & \forall i \notin I, \tilde{\epsilon}_i &= \epsilon_i, & \tilde{z} &= \tilde{s}_I(\tilde{\epsilon}), & \tilde{x} &= g(\tilde{z}). \end{aligned} \quad (1)$$

3.2 Identifiability result

The main theoretical result of this paper is that an LCM \mathcal{M} can be identified from $p(x, \tilde{x})$ up to a relabeling and elementwise transformations of the causal variables:

Theorem 1 (Identifiability of \mathbb{R} -valued LCMs from weak supervision). *Let $\mathcal{M} = \langle \mathcal{C}, \mathcal{X}, g, \mathcal{I}, p_{\mathcal{I}} \rangle$ and $\mathcal{M}' = \langle \mathcal{C}', \mathcal{X}, g', \mathcal{I}', p'_{\mathcal{I}'} \rangle$ be LCMs with the following properties:*

- *The LCMs have an identical observation space \mathcal{X} .*
- *The SCMs \mathcal{C} and \mathcal{C}' both consist of n real-valued endogeneous causal variables and corresponding exogenous noise variables, i. e. $\mathcal{E}_i = \mathcal{Z}_i = \mathcal{Z}'_i = \mathcal{E}'_i = \mathbb{R}$.*
- *The intervention sets \mathcal{I} and \mathcal{I}' consist of all atomic, perfect interventions, $\mathcal{I} = \{\emptyset, \{z_0\}, \dots, \{z_n\}\}$ and similar for \mathcal{I}' .*
- *The intervention distribution $p_{\mathcal{I}}$ and $p'_{\mathcal{I}'}$ have full support.*

Then the following two statements are equivalent:

1. *The LCMs entail equal weakly supervised distributions, $p_{\mathcal{M}}^{\mathcal{X}}(x, \tilde{x}) = p_{\mathcal{M}'}^{\mathcal{X}}(x, \tilde{x})$.*
2. *The LCMs are equivalent in the sense of Def. 2, $\mathcal{M} \sim \mathcal{M}'$.*

Let us summarize the key steps of our proof, which we provide in its entirety in Appendix A.2. The direction $2 \Rightarrow 1$ follows from the definition of equivalence. The direction $1 \Rightarrow 2$ is proven constructively along the following steps:

1. We begin by defining a diffeomorphism $\varphi = g'^{-1} \circ g : \mathcal{Z} \rightarrow \mathcal{Z}'$ and note that if $z, \tilde{z} \sim p_{\mathcal{C}}^{\mathcal{Z}}(z, \tilde{z})$, the weakly supervised distribution of causal variables of model \mathcal{C} , then $\varphi(z), \varphi(\tilde{z}) \sim p_{\mathcal{C}'}^{\mathcal{Z}'}(z', \tilde{z}')$. The distribution over z, \tilde{z} is a mixture, where each intervention target I gives a mixture component; each component is supported on a different $(n+1)$ -dimensional submanifold. Therefore, there exists a bijection between the components $\psi : [n] \rightarrow [n]$ that maps intervention targets I in \mathcal{M} to intervention targets $I' = \psi(I)$ in \mathcal{M}' . Furthermore, because the joint distribution z, \tilde{z} is preserved by φ , first mapping with φ , then intervening, $\mathcal{Z} \xrightarrow{\varphi} \mathcal{Z}' \xrightarrow{I'} \tilde{\mathcal{Z}}'$, equals $\mathcal{Z} \xrightarrow{I} \tilde{\mathcal{Z}} \xrightarrow{\varphi} \tilde{\mathcal{Z}}'$.
2. Because $I = \{i\}$ is a perfect intervention, for the map $\mathcal{Z} \xrightarrow{\varphi} \mathcal{Z}' \xrightarrow{I'} \tilde{\mathcal{Z}}'$, \tilde{z}'_i is independent of z' . Thus, in both maps, \tilde{z}'_i is independent of z . This means that for the path through $\tilde{\mathcal{Z}}$, the intervention sample \tilde{z}_i is transformed into \tilde{z}'_i independently of z . For \mathbb{R} -valued variables, this statistical independence implies that the transformation is constant in z , and thus $\varphi(z)_i$ is constant in z_j for $j \neq i$. φ is therefore an elementwise reparametrization.
3. Using this, we can show that ψ is a causal graph isomorphism and that it is compatible with the causal mechanisms. This proves LCM equivalence $\mathcal{M} \sim \mathcal{M}'$.

4 Practical latent causal models

Theorem 1 means that it is possible to learn causal structure from pixel-level data in the weakly supervised setting. Consider a system that is described by an unknown true LCM and assume that we have access to data pairs (x, \tilde{x}) sampled from its probability density. Then we can train another LCM with learnable components by maximum likelihood. Assuming sufficient data and perfect optimization, this model's density will match that of the ground-truth LCM. Our identifiability result guarantees that the trained LCM then has the same causal variables and causal structure as the ground truth, up to relabelling.

In the following, we describe two neural LCM implementations that can be trained on data.

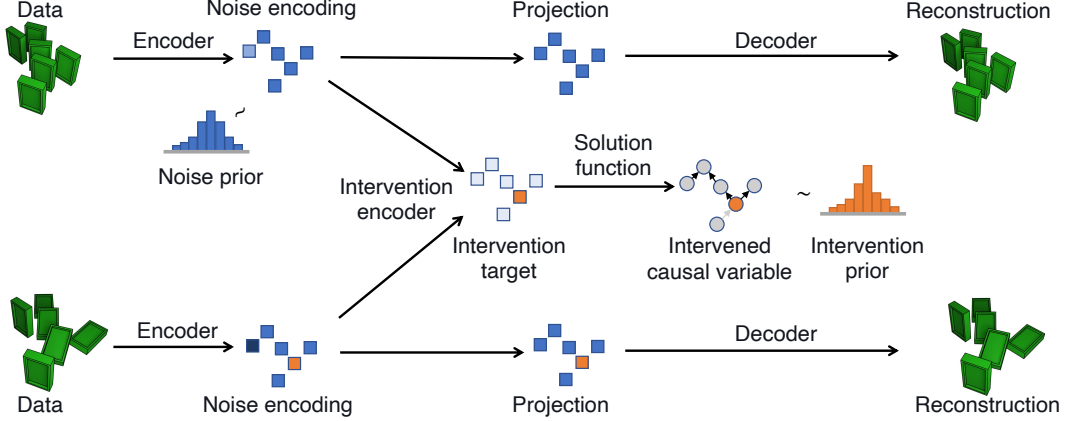


Figure 3: ILCM architecture. Pre- and post-intervention data (left) are encoded to noise encodings and intervention targets, which are then decoded back to the data space. To compute the prior probability density, the noise encodings are transformed into causal variables with the neural solution function.

4.1 Explicit latent causal models (ELCMs)

To implement LCMs with neural networks, we use the variational autoencoder (VAE) framework [4]. We first consider an approach where the causal variables (z, \tilde{z}) are the latent variables. Data (x, \tilde{x}) and latents (z, \tilde{z}) are linked by a stochastic encoder $q(z|x)$ and decoder $p(x|z)$; unlike the deterministic decoder from Sec. 3 this allows us to map high-dimensional data spaces (like images) to low-dimensional causal variables. The causal structure is encoded in the prior $p(z, \tilde{z})$ and consists of a learnable causal graph and learnable causal mechanisms f_i . The first contribution to the prior density is the observational probability density $p(z)$, which factorizes according to the causal graph into components $p(z_i|z_{\text{pa}_i})$, which are given by fixed base densities and the causal mechanisms. The second contribution is the interventional conditional density $p(\tilde{z}|z)$, which is also computable from the graph and causal mechanisms. The model can be trained on the ELBO loss, a variational bound on $-\log p(x, \tilde{x})$. For more details, see Appendix E.

We call this an *explicit latent causal model* (ELCM), as the model directly parameterizes all components of an LCM. In particular, ELCMs contain an explicit representation of the causal graph and causal mechanisms. The graph can be learned by an exhaustive search over all DAGs or through a differentiable DAG parameterization [26–29] and gradient descent.

In our experiments with ELCMs, which we describe in Appendix E, we find that optimally trained ELCMs indeed correctly identify the causal structure and disentangle causal variables on simple datasets. However, jointly learning explicit graph and variable representations presents a challenging optimization problem. In particular, we observe that the loss landscape has local minima corresponding to wrong graph configurations.

4.2 Implicit latent causal models (ILCMs)

To enable causal representation learning in a more robust, scalable way, we propose a second LCM implementation: *Implicit Latent Causal Models* (ILCMs). Like ELCMs, ILCMs are also variational autoencoders with a causally structured prior. The key difference is that ILCMs represent the causal structure through neural solution functions $s(e)$. Under our assumption of diffeomorphic causal mechanisms, the solution function—which maps the vector of noise variables to the causal variables—contains the same information as the causal graph and causal mechanisms that we parameterize with neural networks in ELCMs (see Appendix C). However, unlike ELCMs, this parameterization does not require an explicit graph parameterization. In practice, ILCMs are thus easier to train than ELCMs.

Latents The latent variables in an ILCMs are *noise encodings*, defined through the inverse solution function as $e = s^{-1}(z)$ and $\tilde{e} = s^{-1}(\tilde{z})$. The pre-intervention noise encoding e is identical to the SCM noise variables. The post-intervention noise encoding \tilde{e} corresponds to the value of the SCM noise variables that would have generated the post-intervention causal variables \tilde{z} under the

unintervened SCM mechanisms. ILCMs contain a stochastic encoder $q(e|x)$ and decoder $p(x|e)$ that map data (x, \tilde{x}) to noise encodings (e, \tilde{e}) .

Noise encodings have the convenient property that under an intervention with intervention targets I , precisely the components e_I change value: $e_i \neq \tilde{e}_i \Leftrightarrow i \in I$ with probability 1. We prove this property in Appendix A. This means that from noise encodings e, \tilde{e} , we can infer interventions easily. We use a simple heuristic intervention encoder that assigns higher intervention probability $q(i \in I|x, \tilde{x})$ to a component i the more this component of the noise encoding changes under interventions:

$$\log q(i \in I|x, \tilde{x}) \sim h(\mu_e(x)_i - \mu_e(\tilde{x})_i), \quad (2)$$

where $\mu_e(x)$ is the mean function of the noise encoder $q(e|x)$ and h is a quadratic function with learnable parameters. Both the equality pattern of e under interventions and this heuristic intervention encoder are similar to the ones used for disentangled representation learning in Ref. [5].

Prior Given encoders for noise encodings and intervention targets, let us now write down the prior $p(e, \tilde{e}, I)$, which encodes the structure of the weakly supervised setting. The intervention-target prior $p(I)$ and the pre-intervention noise distribution $p(e)$ are given by simple base densities, which we choose as uniform categorical and standard Gaussian, respectively. The post-intervention noise encodings \tilde{e} follow the conditional probability distribution

$$p(\tilde{e}|e, I) = \prod_{i \notin I} \delta(\tilde{e}_i - e_i) \prod_{i \in I} p(\tilde{e}_i|e) = \prod_{i \notin I} \delta(\tilde{e}_i - e_i) \prod_{i \in I} \tilde{p}(\tilde{z}_i) \left| \frac{\partial \tilde{z}_i}{\partial \tilde{e}_i} \right|, \quad \tilde{z}_i = \bar{s}_i(\tilde{e}_i; e_{\setminus i}). \quad (3)$$

In the second equality we have parameterized the conditional density $p(\tilde{e}_i|e)$ with a conditional normalizing flow consisting of a learnable diffeomorphic transformation $\tilde{e}_i \mapsto \tilde{z}_i = \bar{s}_i(\tilde{e}_i; e_{\setminus i})$ and a base density \tilde{p} on \tilde{z}_i , which we choose as standard Gaussian.

How does this prior encode causal structure? We rely on three key properties of SCMs, shown in Appendix A: 1) the noise variables e_i are independent of each other; 2) upon intervening on variable i , the post-intervention causal variable \tilde{z}_i are independent of all e_j ; 3) while for the other variables $j \neq i$, the noise encodings are unchanged $\tilde{e}_j = e_j$. These three properties are ensured in the ILCM prior in Eq. (3). We show in Appendix C that therefore each ILCM is equivalent to a unique ELCM. For each variable i , the ILCM function \bar{s}_i is equal to the solution function s_i of the equivalent ELCM, which maps from noise variables to causal variable z_i .

Thus, by learning to transform \tilde{e}_i into $\tilde{z}_i = \bar{s}_i(\tilde{e}_i; e)$ in the ILCM, we learn the solution function of the corresponding ELCM. This implicitly describes both the causal graph and the causal mechanisms f_i . We can thus learn a causal model without ever explicitly modelling a graph.⁵

The final question is how to implement the first terms in Eq. (3), which encode that those noise encodings that are not part of the intervention targets I should not change value under the intervention. We enforce this in the encoder by setting the non-intervention components of e and \tilde{e} to the same value [similar to 5]. In Appendix C this procedure is described in more detail. We will refer to this projective noise encoder as $q(e, \tilde{e}|x, \tilde{x}, I)$.

Learning Putting everything together, an ILCM consists of an intervention encoder $q(I|x, \tilde{x})$, a noise encoder $q(e, \tilde{e}|x, \tilde{x}, I)$, a noise decoder $p(x|e)$, and transformations / solution functions $s_i(\cdot; e)$, see Fig. 3. All of these components are implemented with neural networks and learnable, see Appendix C for details. The lower bound on the joint log likelihood of pre-intervention and post-intervention data is given by

$$\log p(x, \tilde{x}) \geq \mathbb{E}_{I \sim q(I|x, \tilde{x})} \mathbb{E}_{e, \tilde{e} \sim q(e, \tilde{e}|x, \tilde{x}, I)} \left[\log p(I) + \log p(e) + \log p(\tilde{e}|e, I) - \log q(I|x, \tilde{x}) - \log q(e, \tilde{e}|x, \tilde{x}, I) + \log p(x|e) + \log p(\tilde{x}|\tilde{e}) \right]. \quad (4)$$

⁵The solution function of an ELCM only depends on ancestors in the graph. The learned transformation $s_i(e_i; e_{\setminus i})$ of an ILCM should thus also depend only on ancestors of i . As each s_i is constructed to be a diffeomorphism in its first argument, jointly they have a triangular structure and thus a diffeomorphism $s : e \mapsto z$. In practice, however, the learned solution functions may still depend weakly on non-ancestors. Therefore, to ensure that s always forms a diffeomorphism, at some point in training, we test functional dependence to infer ancestral dependence, pick a topological ordering of variables conforming to the ancestry, and parameterize the solution functions s_i to only depend on earlier variables in the ordering.

The model is trained by minimizing the corresponding VAE loss, learning to map low-level data to noise variables (with q) and to map noise variables to causal variables (with s). The expectation over I is computed via summation, but could alternatively be done with sampling.

In practice, we find it beneficial to add a regularization term to the loss that disincentivizes collapse to a lower-dimensional submanifold of the latent space. For each batch of training data, we compute the batch-aggregate intervention posterior $q_I(I) = \mathbb{E}_{x, \tilde{x} \in \text{batch}} [q(I|x, \tilde{x})]$. To the beta-VAE loss we then add the negative entropy of this distribution, weighted with a hyperparameter.

Downstream tasks Despite the implicit representation of causal structure, we argue that ILCMs let us solve various tasks:

- *Causal representation learning / disentanglement*: ILCMs allow us to map low-level data x to causal variables z by applying the encoder q followed by the solution functions s .
- *Intervention inference*: It is also straightforward to infer intervention targets from an observed pair (x, \tilde{x}) of pre-intervention and post-intervention data, as this just requires evaluating the intervention-target encoder $q_I(x, \tilde{x})$.
- *Causal discovery / identification*: We propose two methods to infer the causal graphs after training an ILCM. One is to use an off-the-shelf method for causal discovery on the learned representations. Since the ILCM allows us to infer intervention targets, we can use intervention-based algorithms. In this paper, we use ENCO [28], a recent differentiable causal discovery method that exploits interventions to obtain acyclic graphs without requiring constrained optimization. Alternatives to ENCO include DCDI [27] and GIES [30]. Alternatively, we can analyze the causal structure implicitly represented in the learned solution functions s_i . We propose a heuristic algorithm that proceeds in three steps. First, it infers the topological order by sorting variables such that s_i only depends on e_j if z_i is after z_j in the topological order. It then iteratively rewrites the solution functions such that they only depend on ancestors in the topological order. Finally, it determines which causal ancestors are direct parents by testing the functional dependence of the causal mechanisms. We describe this algorithm in more detail in Appendix C.
- *Generation of interventions and counterfactuals*: The ILCM entails a generative model for pairs of pre- and post-intervention data. It is straightforward to sample from the joint distribution $p(x, \tilde{x}, I)$, from the conditional $p(x, \tilde{x}|I)$, or from the conditional $p(\tilde{x}|x, I)$.

5 Experiments

Finally, we demonstrate latent causal models in practice. Here we focus on implicit LCMs; explicit LCMs are demonstrated in similar experiments in Appendix E. We evaluate the causal graphs learned by the ILCM models either with ENCO (ILCM-E) or with the heuristic algorithm described above (ILCM-H).

Baselines Since we are to the best of our knowledge the first to study causal representation learning in this weakly supervised setting, we are not aware of any baseline methods designed for this task. We nevertheless compare ILCMs to three other methods. First, we define a *disentanglement VAE* that models the weakly supervised process, but assumes independent factors of variation rather than a non-trivial causal structure between the variables. This baseline is similar to the method proposed by Ref. [5], but it differs in some implementation details to be more comparable to our ILCM setup. We infer the causal graph between the learned representations with ENCO (dVAE-E). We also compare to an unstructured β -VAE that treats x and \tilde{x} as i. i. d. and uses a standard Gaussian prior. Finally, for the pixel-level data, we consider a slot attention model [31], which segments the image unsupervisedly into as many objects as there are causal variables. The latent representation associated to each object is considered a learned causal variable.

5.1 2D toy experiment

We first demonstrate LCMs in a pedagogical toy experiment with $\mathcal{X} = \mathcal{Z} = \mathbb{R}^2$. Training data is generated from a nonlinear SCM with the graph $z_1 \rightarrow z_2$ and mapped to the data space through a randomly initialized normalizing flow.

An ILCM trained in the weakly supervised setting is able to reconstruct the causal factors accurately up

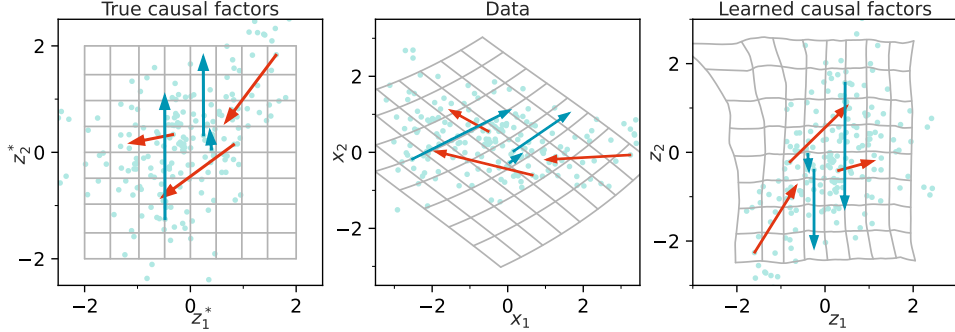


Figure 4: 2D toy data with graph $z_1^* \rightarrow z_2^*$. The grey grids show the map between true causal factors, data, and latent causal factors learned by the LCM. The mint dots indicate the observational data distribution, the arrows from z to \tilde{z} show interventions targeting z_1^* (red) or z_2^* (blue). The fact that axis-aligned lines in the true latent space are mapped to axis-aligned lines in the learned latent space implies that the disentanglement succeeded.

to elementwise reparameterizations, as shown in Fig. 4. In Tbl. 1 we quantify the quality of the learned representations with the DCI disentanglement score [32]. We find that our LCM is able to disentangle the causal factors almost perfectly, while the baselines, which assume independent factors of variation, fail as expected. Both the ILCM and the dVAE baseline infer the intervention targets with high accuracy. Finally, we test the quality of the learned causal graphs. We infer the implicit graph with ENCO and the heuristic algorithm discussed above. In both cases, the learned causal graph is identical to the correct one, whereas the representations found by the dVAE baseline induce a wrong graph.

5.2 Causal3DIdent

We then turn to pixel-level data and more complex causal graphs. We test ILCMs on an adaptation of the Causal3DIdent dataset [14], which contains images of three-dimensional objects under variable positions and lighting conditions. We consider three causal variables representing object hue, the spotlight hue, and the position of the spotlight. We construct six versions of this dataset, each with a different causal graph, randomly initialized nonlinear structure functions, and heteroskedastic noise. These are mapped to images with a resolution of 64×64 , see Fig. 5 for examples.

ILCMs are again able to disentangle the causal variables reliably. The results in Tbl. 1 show that the learned representations are more disentangled than those learned by methods that do not account for causal structure. The LCM as well as the dVAE baseline can infer interventions with almost perfect accuracy. We demonstrate this in Fig. 5 by comparing true and inferred interventions, see Appendix D.3 for details. The ILCMs also learn the causal graphs accurately, while the acausal dVAE-E baseline does in most cases not find the correct causal graphs.

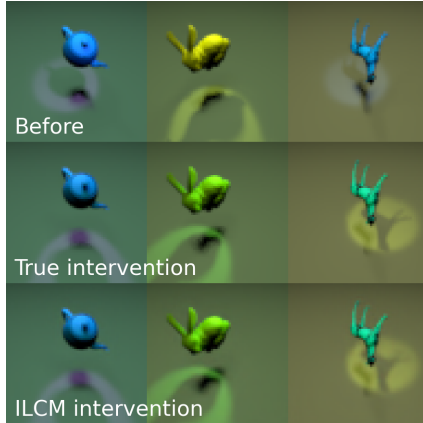


Figure 5: Causal3DIdent before (top) and after (middle) interventions, and post-intervention samples generated from the ILCM under the intervention inferred from the data (bottom), indicating we correctly learned to intervene.

5.3 CausalCircuit

While Causal3DIdent provides a good test of the ability to disentangle features that materialize in pixel space in different ways, like through the position of lights and the color of objects, the underlying causal structure we imposed may feel rather ad-hoc. To explore causal representation learning in a more intuitively causal setting, we introduce a new dataset, which we call CausalCircuit.

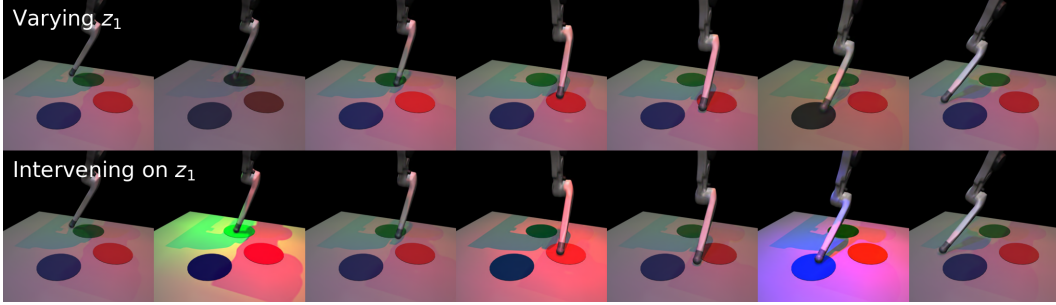


Figure 6: Varying learned causal factors vs. intervening on them. With a trained ILCM, we encode a single test image (left column). In the top row, we then vary the latent z_1 independently, without computing causal effects, and show the corresponding reconstructed images. Only the robot arm position changes, highlighting that we learned a disentangled representation. In the bottom row we instead *intervene* on z_1 and observe the causal effects: the robot arm may activate lights, which in turn can affect other lights in the circuit.

The CausalCircuit system consists of a robot arm that can interact with multiple touch-sensitive lights. The lights are connected with a stochastic circuit: a light is more likely to be on if its button is pressed or if its parent lights are on. The robot arm itself can be seen as part of the causal system. Concretely, we consider the causal graph shown in Fig. 7. This system is observed from a fixed-position camera, and we generate samples in $512 \times 512 \times 3$ resolution with MuJoCo [33], see Appendix D for more details.

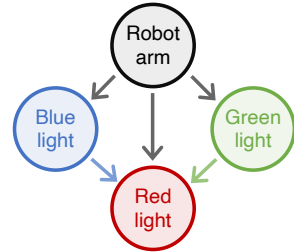


Figure 7: Causal graph of the CausalCircuit dataset.

ILCMs are again able to disentangle the causal variables reliably and better than the acausal baselines, see Tbl. 1. As shown in Appendix D, the slot attention model fails because the lights have no limited spatial extent and thus are not well represented by segments of the image. Interventions are identified with high accuracy. ILCMs also correctly learn the causal graph shown in Fig. 6, both when extracted with ENCO and with our heuristic algorithm. In Fig. 6 we demonstrate how ILCMs let us infer and manipulate causal factors and reason about interventions.

By studying variations of this dataset, we tested the limitations of our method. We find that it works reliably only as long as the causal variables are continuous (that is, when we model the lights with a continuous intensity). As soon as we consider discrete states, the assumptions of our identifiability theorem are violated and the model has difficulty disentangling these variables.

5.4 Scaling with graph size

Finally, we study how LCMs scale with the size of the causal system. We generate simple synthetic datasets with $\mathcal{X} = \mathcal{Z} = \mathbb{R}^n$. For each dimension n , we generate three datasets, using linear SCMs with random DAGs, in which each edge in a fixed topological order is sampled from a Bernoulli distribution with probability 0.5. The causal variables are mapped to the data space through a randomly sampled $SO(n)$ rotation.

We find that ILCMs are able to reliably disentangle the causal variables in systems with up to approximately 10 causal variables, see Fig. 8. In this regime, the true causal graphs are also identified with good accuracy, see Appendix D.5. In larger causal systems, both disentanglement and graph accuracy become worse; more work is required to improve the scaling of our approach to causal representation learning.

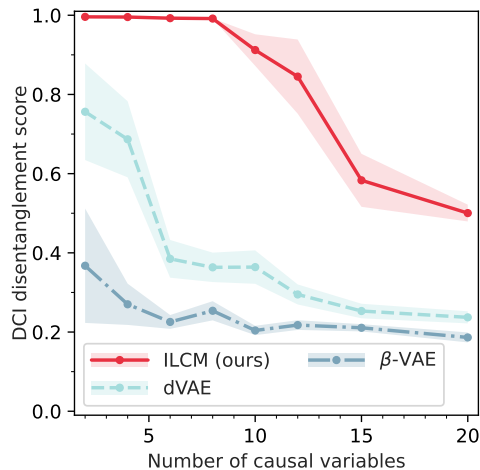


Figure 8: Scaling with graph size. LCMs disentangle causal variables robustly in simple systems with up to ~ 10 causal variables.

6 Discussion

What makes a variable causal? One school of thought is that it that causal variables are those aspects of a system that can be intervened upon [34]. Following this logic, we find it interesting to ask: can we uniquely determine the causal variables underlying a system just by observing the effect of interventions?

In this work we have found a partial answer to this question: we have shown in theory and practice that under certain assumptions, causal variables and their causal structure are identifiable from low-level representations like the pixels of a camera feed if the system is observed before and after random, unlabeled interventions. Our identifiability theorem extends the results by Locatello et al. [5] from independent factors of variation (trivial causal graphs) to arbitrary causal graphs.

Latent causal structure can be described in a variational autoencoder setup. However, a straightforward, explicit parameterization of the causal structure requires simultaneously learning the variables and the causal graph. We found that leads to challenging optimization problems, especially when scaling to larger systems. As a more robust alternative, we introduced implicit latent causal models (ILCMs), which parameterize causal structure without requiring an explicit graph representation. We also discussed two algorithms for extracting the learned causal mechanisms and graph after training.

In first experiments, we demonstrated that ILCMs let us reliably disentangle causal factors, identify causal graphs, and infer interventions from unstructured pixel data. For these experiments, we introduced the new CausalCircuit dataset, which consists of images of a robot arm interacting with connected switches and lights.

The setting we consider is motivated by a potentially useful scenario: learning causal structure from passive observations of an agent (or demonstrator) interacting with a causal system. However, it is currently far from practical. Our identifiability result relies on a number of assumptions, including that interventions are stochastic and perfect, that all atomic interventions may be observed, and that the causal variables are real-valued. In addition, realistic temporal sequence data are not likely to exactly correspond to a causal system before and after an intervention (while preserving the noise variables); whether our causal abstraction provides a useful approximation remains to be tested. We discuss these requirements and their potential relaxation in Appendix B. Similarly, our practical implementation has so far been restricted to simplified datasets with relatively few, continuous causal variables, and when trying to relax these limitations we saw the model performance decrease quickly. While more work will be required to make latent causal models applicable to real-world settings, we believe that our results demonstrate that causal representation learning is possible without explicit labels.

Acknowledgments We want to thank Joey Bose, Thomas Kipf, Dominik Neuenfeld, and Frank Rösler for useful discussions and Gabriele Cesa, Yang Yang, and Yunfan Zhang for helping with our experiments.

Table 1: Experiment results. We compare our ILCM-E (using ENCO for graph inference) and ILCM-H (with a heuristic for graph inference) to disentanglement VAE (dVAE-E), unstructured β -VAE, and slot attention baselines. We show the DCI disentanglement score (D), the accuracy of intervention inference (Acc), and structural Hamming distance (SHD) between learned and true graph. Best results in bold.

Dataset	Method	D	Acc	SHD
2D toy data	ILCM-E (ours)	0.99	0.96	0.00
	ILCM-H (ours)	0.99	0.96	0.00
	dVAE-E	0.35	0.96	1.00
	β -VAE	0.52	-	-
Causal3DIdent	ILCM-E (ours)	0.99	0.98	0.00
	ILCM-H (ours)	0.99	0.98	0.17
	dVAE-E	0.82	0.98	1.67
	β -VAE	0.66	-	-
	Slot attention	0.60	-	-
CausalCircuit	ILCM-E (ours)	0.97	1.00	0.00
	ILCM-H (ours)	0.97	1.00	0.00
	dVAE-E	0.34	1.00	5.00
	β -VAE	0.39	-	-
	Slot attention	0.38	-	-

References

- [1] Bernhard Schölkopf, Francesco Locatello, Stefan Bauer, Nan Rosemary Ke, Nal Kalchbrenner, Anirudh Goyal, and Yoshua Bengio. Toward causal representation learning. *Proceedings of the IEEE*, 109(5):612–634, 2021.
- [2] Frederick Eberhardt. Green and grue causal variables. *Synthese*, 193(4):1029–1046, 2016.
- [3] Francesco Locatello, Stefan Bauer, Mario Lucic, Gunnar Raetsch, Sylvain Gelly, Bernhard Schölkopf, and Olivier Bachem. Challenging common assumptions in the unsupervised learning of disentangled representations. In Kamalika Chaudhuri and Ruslan Salakhutdinov, editors, *Proceedings of the 36th International Conference on Machine Learning*, volume 97 of *Proceedings of Machine Learning Research*, pages 4114–4124. PMLR, 2019.
- [4] Diederik P. Kingma and Max Welling. Auto-Encoding Variational Bayes. In *2nd International Conference on Learning Representations, ICLR 2014, Banff, AB, Canada, April 14-16, 2014, Conference Track Proceedings*, 2014.
- [5] Francesco Locatello, Ben Poole, Gunnar Rätsch, Bernhard Schölkopf, Olivier Bachem, and Michael Tschannen. Weakly-supervised disentanglement without compromises. In *International Conference on Machine Learning*, pages 6348–6359. PMLR, 2020.
- [6] Aapo Hyvärinen and Erkki Oja. Independent component analysis: algorithms and applications. *Neural Networks*, 13:411–430, 2000.
- [7] Rui Shu, Yining Chen, Abhishek Kumar, Stefano Ermon, and Ben Poole. Weakly Supervised Disentanglement with Guarantees. In *International Conference on Learning Representations*, 2020.
- [8] Ilyes Khemakhem, Diederik Kingma, Ricardo Monti, and Aapo Hyvarinen. Variational Autoencoders and Nonlinear ICA: A Unifying Framework. In Silvia Chiappa and Roberto Calandra, editors, *Proceedings of the Twenty Third International Conference on Artificial Intelligence and Statistics*, volume 108 of *Proceedings of Machine Learning Research*, pages 2207–2217. PMLR, 2020.
- [9] Hermanni Hälvä, Sylvain Le Corff, Luc Lehéricy, Jonathan So, Yongjie Zhu, Elisabeth Gassiat, and Aapo Hyvarinen. Disentangling Identifiable Features from Noisy Data with Structured Nonlinear ICA. In A. Beygelzimer, Y. Dauphin, P. Liang, and J. Wortman Vaughan, editors, *Advances in Neural Information Processing Systems*, 2021.
- [10] Luigi Gresele, Julius von Kügelgen, Vincent Stimper, Bernhard Schölkopf, and Michel Besserve. Independent mechanism analysis, a new concept? In A. Beygelzimer, Y. Dauphin, P. Liang, and J. Wortman Vaughan, editors, *Advances in Neural Information Processing Systems*, 2021.
- [11] Weiran Yao, Yuewen Sun, Alex Ho, Changyin Sun, and Kun Zhang. Learning Temporally Causal Latent Processes from General Temporal Data. In *International Conference on Learning Representations*, 2022.
- [12] Sebastien Lachapelle, Pau Rodriguez, Rémi Le, Yash Sharma, Katie E Everett, Alexandre Lacoste, and Simon Lacoste-Julien. Disentanglement via Mechanism Sparsity Regularization: A New Principle for Nonlinear ICA. In *First Conference on Causal Learning and Reasoning*, 2022.
- [13] Chaochao Lu, Yuhuai Wu, José Miguel Hernández-Lobato, and Bernhard Schölkopf. Nonlinear invariant risk minimization: A causal approach. *arXiv preprint arXiv:2102.12353*, 2021.
- [14] Julius von Kügelgen, Yash Sharma, Luigi Gresele, Wieland Brendel, Bernhard Schölkopf, Michel Besserve, and Francesco Locatello. Self-Supervised Learning with Data Augmentations Provably Isolates Content from Style. In *Thirty-Fifth Conference on Neural Information Processing Systems*, 2021.
- [15] Phillip Lippe, Sara Magliacane, Sindy Löwe, Yuki M. Asano, Taco Cohen, and Efstratios Gavves. CITRIS: Causal Identifiability from Temporal Intervened Sequences. In *Proceedings of the 39th International Conference on Machine Learning, ICML, 2022*.
- [16] Mengyue Yang, Furuo Liu, Zhitang Chen, Xinwei Shen, Jianye Hao, and Jun Wang. CausalVAE: Disentangled representation learning via neural structural causal models. In *Proceedings of the IEEE/CVF Conference on Computer Vision and Pattern Recognition*, pages 9593–9602, 2021.
- [17] Jeffrey Adams, Niels Hansen, and Kun Zhang. Identification of partially observed linear causal models: Graphical conditions for the non-gaussian and heterogeneous cases. In

- M. Ranzato, A. Beygelzimer, Y. Dauphin, P.S. Liang, and J. Wortman Vaughan, editors, *Advances in Neural Information Processing Systems*, volume 34, pages 22822–22833. Curran Associates, Inc., 2021. URL <https://proceedings.neurips.cc/paper/2021/file/c0f6fb5d3a389de216345e490469145e-Paper.pdf>.
- [18] Feng Xie, Ruichu Cai, Biwei Huang, Clark Glymour, Zhifeng Hao, and Kun Zhang. Generalized independent noise condition for estimating latent variable causal graphs. In H. Larochelle, M. Ranzato, R. Hadsell, M.F. Balcan, and H. Lin, editors, *Advances in Neural Information Processing Systems*, volume 33, pages 14891–14902. Curran Associates, Inc., 2020. URL <https://proceedings.neurips.cc/paper/2020/file/aa475604668730af60a0a87cc92604da-Paper.pdf>.
- [19] Bohdan Kivva, Goutham Rajendran, Pradeep Ravikumar, and Bryon Aragam. Learning latent causal graphs via mixture oracles. In M. Ranzato, A. Beygelzimer, Y. Dauphin, P.S. Liang, and J. Wortman Vaughan, editors, *Advances in Neural Information Processing Systems*, volume 34, pages 18087–18101. Curran Associates, Inc., 2021. URL <https://proceedings.neurips.cc/paper/2021/file/966aad8981dcc75b5b8ab04427a833b2-Paper.pdf>.
- [20] Krzysztof Chalupka, Pietro Perona, and Frederick Eberhardt. Visual causal feature learning. *Uncertainty in Artificial Intelligence*, December 2014.
- [21] Sander Beckers and Joseph Y Halpern. Abstracting causal models. *Proc. Conf. AAAI Artif. Intell.*, 33:2678–2685, July 2019.
- [22] Jonas Peters, Dominik Janzing, and Bernhard Schölkopf. *Elements of causal inference: foundations and learning algorithms*. The MIT Press, 2017.
- [23] Paul K Rubenstein, Sebastian Weichwald, Stephan Bongers, Joris M Mooij, Dominik Janzing, Moritz Grosse-Wentrup, and Bernhard Schölkopf. Causal consistency of structural equation models. *Uncertainty in Artificial Intelligence*, July 2017.
- [24] Judea Pearl. *Causality : models, reasoning, and inference*. Cambridge University Press, Cambridge, U.K. New York, 2000. ISBN 978-0521895606.
- [25] Stephan Bongers, Patrick Forré, Jonas Peters, and Joris M. Mooij. Foundations of Structural Causal Models with Cycles and Latent Variables. *Annals of Statistics*, 49(5):2885–2915, 2021. doi: 10.1214/21-AOS2064.
- [26] Eric Jang, Shixiang Gu, and Ben Poole. Categorical Reparameterization with Gumbel-Softmax. In *5th International Conference on Learning Representations, ICLR 2017, Toulon, France, April 24-26, 2017, Conference Track Proceedings*, 2017.
- [27] Philippe Brouillard, Sébastien Lachapelle, Alexandre Lacoste, Simon Lacoste-Julien, and Alexandre Drouin. Differentiable Causal Discovery from Interventional Data. In Hugo Larochelle, Marc’ Aurelio Ranzato, Raia Hadsell, Maria-Florina Balcan, and Hsuan-Tien Lin, editors, *Advances in Neural Information Processing Systems 33: Annual Conference on Neural Information Processing Systems 2020, NeurIPS 2020, December 6-12, 2020, virtual*, 2020.
- [28] Phillip Lippe, Taco Cohen, and Efstratios Gavves. Efficient Neural Causal Discovery without Acyclicity Constraints. In *International Conference on Learning Representations*, 2022.
- [29] Bertrand Charpentier, Simon Kibler, and Stephan Günnemann. Differentiable DAG sampling. March 2022.
- [30] Alain Hauser and Peter Bühlmann. Characterization and Greedy Learning of Interventional Markov Equivalence Classes of Directed Acyclic Graphs. *Journal of Machine Learning Research*, 13(1):2409–2464, 2012. ISSN 1532-4435.
- [31] Francesco Locatello, Dirk Weissenborn, Thomas Unterthiner, Aravindh Mahendran, Georg Heigold, Jakob Uszkoreit, Alexey Dosovitskiy, and Thomas Kipf. Object-centric learning with slot attention. *Advances in Neural Information Processing Systems*, 33:11525–11538, 2020.
- [32] Cian Eastwood and Christopher K I Williams. A framework for the quantitative evaluation of disentangled representations. *International Conference on Learning Representations*, February 2018.
- [33] Emanuel Todorov, Tom Erez, and Yuval Tassa. MuJoCo: A physics engine for model-based control. In *2012 IEEE/RSJ International Conference on Intelligent Robots and Systems*, pages 5026–5033, October 2012.

- [34] James Woodward. *Making Things Happen: A Theory of Causal Explanation*. Oxford University Press, USA, October 2005.
- [35] Stack Exchange user zhw. Lebesgue measure-preserving differentiable function. Mathematics Stack Exchange, 2016. URL <https://math.stackexchange.com/q/1755585>. (version: 2016-04-23).
- [36] Tobias Fritz. A synthetic approach to markov kernels, conditional independence and theorems on sufficient statistics. *Advances in Mathematics*, 370:107239, 2020. ISSN 0001-8708. doi: <https://doi.org/10.1016/j.aim.2020.107239>. URL <https://www.sciencedirect.com/science/article/pii/S0001870820302656>.
- [37] Brendan Fong. Causal theories: A categorical perspective on bayesian networks. *arXiv preprint arXiv:1301.6201*, 2013.
- [38] Emily Riehl. *Category Theory in Context*. Aurora: Dover Modern Math Originals. Dover Publications, 2017. ISBN 9780486820804.
- [39] Diederik P. Kingma and Jimmy Ba. Adam: A Method for Stochastic Optimization. In Yoshua Bengio and Yann LeCun, editors, *3rd International Conference on Learning Representations, ICLR 2015, San Diego, CA, USA, May 7-9, 2015, Conference Track Proceedings*, 2015.
- [40] Ilya Loshchilov and Frank Hutter. SGDR: Stochastic gradient descent with warm restarts. August 2016.
- [41] Thomas Kipf, Gamaleldin F Elsayed, Aravindh Mahendran, Austin Stone, Sara Sabour, Georg Heigold, Rico Jonschkowski, Alexey Dosovitskiy, and Klaus Greff. Conditional object-centric learning from video. *arXiv preprint arXiv:2111.12594*, 2021.
- [42] F. Pedregosa, G. Varoquaux, A. Gramfort, V. Michel, B. Thirion, O. Grisel, M. Blondel, P. Prettenhofer, R. Weiss, V. Dubourg, J. Vanderplas, A. Passos, D. Cournapeau, M. Brucher, M. Perrot, and E. Duchesnay. Scikit-learn: Machine learning in Python. *Journal of Machine Learning Research*, 12:2825–2830, 2011.
- [43] Blender Online Community. *Blender - a 3D modelling and rendering package*. Blender Foundation, Stichting Blender Foundation, Amsterdam, 2021. <http://www.blender.org>.
- [44] Martin Edward Newell. *The Utilization of Procedure Models in Digital Image Synthesis*. PhD thesis, The University of Utah, 1975. AAI7529894.
- [45] Venkat Krishnamurthy and Marc Levoy. Fitting Smooth Surfaces to Dense Polygon Meshes. In *Proceedings of the 23rd Annual Conference on Computer Graphics and Interactive Techniques, SIGGRAPH '96*, page 313–324, New York, NY, USA, 1996. Association for Computing Machinery. ISBN 0897917464. doi: 10.1145/237170.237270.
- [46] Greg Turk and Marc Levoy. Zippered Polygon Meshes from Range Images. In *Proceedings of the 21st Annual Conference on Computer Graphics and Interactive Techniques, SIGGRAPH '94*, page 311–318, New York, NY, USA, 1994. Association for Computing Machinery. ISBN 0897916670. doi: 10.1145/192161.192241.
- [47] Keenan Crane. Keenan’s 3D Model Repository. <https://www.cs.cmu.edu/~kmcraane/Projects/ModelRepository/>, 2021.
- [48] Brian Curless and Marc Levoy. A Volumetric Method for Building Complex Models from Range Images. In *Proceedings of the 23rd Annual Conference on Computer Graphics and Interactive Techniques, SIGGRAPH '96*, page 303–312, New York, NY, USA, 1996. Association for Computing Machinery. ISBN 0897917464. doi: 10.1145/237170.237269.
- [49] Emil Praun, Adam Finkelstein, and Hugues Hoppe. Lapped Textures. In *Proceedings of ACM SIGGRAPH 2000*, pages 465–470, July 2000.
- [50] Manuel Wüthrich, Felix Widmaier, Felix Grimmering, Joel Akpo, Shruti Joshi, Vaibhav Agrawal, Bilal Hammoud, Majid Khadiv, Miroslav Bogdanovic, Vincent Berenz, et al. Trifinger: An open-source robot for learning dexterity. *arXiv preprint arXiv:2008.03596*, 2020.
- [51] Xun Zheng, Bryon Aragam, Pradeep Ravikumar, and Eric P. Xing. DAGs with NO TEARS: Continuous Optimization for Structure Learning. In Samy Bengio, Hanna M. Wallach, Hugo Larochelle, Kristen Grauman, Nicolò Cesa-Bianchi, and Roman Garnett, editors, *Advances in Neural Information Processing Systems 31: Annual Conference on Neural Information Processing Systems 2018, NeurIPS 2018, December 3-8, 2018, Montréal, Canada*, pages 9492–9503, 2018.

Checklist

1. For all authors...
 - (a) Do the main claims made in the abstract and introduction accurately reflect the paper’s contributions and scope? **[Yes]**
 - (b) Did you describe the limitations of your work? **[Yes]** We strive to be transparent about the limitations of our work. In the theory section we list the assumptions, in the experiment section we discuss observed failures, and in the conclusions and in Appendix B we discuss the requirements of our approach again.
 - (c) Did you discuss any potential negative societal impacts of your work? **[Yes]** See Appendix F.
 - (d) Have you read the ethics review guidelines and ensured that your paper conforms to them? **[Yes]**
2. If you are including theoretical results...
 - (a) Did you state the full set of assumptions of all theoretical results? **[Yes]** We provide our list of assumptions in Sec. 5 and Appendix A and further discuss them in Appendix B.
 - (b) Did you include complete proofs of all theoretical results? **[Yes]** Our identifiability theorem is proven in Appendix A.
3. If you ran experiments...
 - (a) Did you include the code, data, and instructions needed to reproduce the main experimental results (either in the supplemental material or as a URL)? **[No]** Not yet, but we aim to publish them as soon as we obtain approval to do so.
 - (b) Did you specify all the training details (e.g., data splits, hyperparameters, how they were chosen)? **[Yes]** We provide these details in Appendix D.
 - (c) Did you report error bars (e.g., with respect to the random seed after running experiments multiple times)? **[No]**
 - (d) Did you include the total amount of compute and the type of resources used (e.g., type of GPUs, internal cluster, or cloud provider)? **[No]**
4. If you are using existing assets (e.g., code, data, models) or curating/releasing new assets...
 - (a) If your work uses existing assets, did you cite the creators? **[Yes]** We use the Causal3DIdent dataset from von Kügelgen et al. [14].
 - (b) Did you mention the license of the assets? **[No]**
 - (c) Did you include any new assets either in the supplemental material or as a URL? **[No]** We strive to publish our CausalCircuit dataset as soon as possible.
 - (d) Did you discuss whether and how consent was obtained from people whose data you’re using/curating? **[N/A]** We only consider synthetic data showing simulated objects.
 - (e) Did you discuss whether the data you are using/curating contains personally identifiable information or offensive content? **[N/A]**
5. If you used crowdsourcing or conducted research with human subjects...
 - (a) Did you include the full text of instructions given to participants and screenshots, if applicable? **[N/A]**
 - (b) Did you describe any potential participant risks, with links to Institutional Review Board (IRB) approvals, if applicable? **[N/A]**
 - (c) Did you include the estimated hourly wage paid to participants and the total amount spent on participant compensation? **[N/A]**

Appendices

In the following we provide additional results and details that did not fit into our main paper. In Appendix A we provide precise definitions and a complete proof of our identifiability theorem. We then discuss the assumptions underlying this result and their generalization in Appendix B. Appendix C covers implicit latent causal models (ILCMs) and their training, while Appendix D provides details for our experiments. In Appendix E we describe explicit latent causal models (ELCMs) and our experiments with them. Finally, in Appendix F we discuss the potential societal impact of our work.

A Identifiability result

A.1 Definitions

Here we define objects and relations that were not formally defined in the main body of the paper, but are necessary to make Thm. 1 precise and to prove it.

We use the following notation:

- $[n] = \{1, \dots, n\}$
- $\text{pa}_i^{\mathcal{C}} \subseteq [n]$ the set of parent nodes of node i in graph $\mathcal{G}(\mathcal{C})$.
- $\text{desc}_i^{\mathcal{C}} \subseteq [n]$ the set of descendant nodes of node i in graph $\mathcal{G}(\mathcal{C})$, excluding i itself.
- $\text{anc}_i^{\mathcal{C}} \subseteq [n]$ the set of ancestor nodes of node i in graph $\mathcal{G}(\mathcal{C})$, excluding i itself.
- $\text{nonanc}_i^{\mathcal{C}} = [n] \setminus (\text{anc}_i^{\mathcal{C}} \cup \{i\})$ the set of non-ancestor nodes of node i in graph $\mathcal{G}(\mathcal{C})$, excluding i itself.
- Given measure p on space A and measurable function $f : A \rightarrow B$, f_*p is the push-forward measure on B .

We describe causal structure with SCMs.

Definition 4 (Structural causal model (SCM)). *An SCM is a tuple $\mathcal{C} = \langle \mathcal{Z}, \mathcal{E}, F, p_{\mathcal{E}} \rangle$ consisting of the following:*

- domains $\mathcal{Z} = \mathcal{Z}_1 \times \dots \times \mathcal{Z}_n$ of causal (endogenous) variables z_1, \dots, z_n ;
- domains $\mathcal{E} = \mathcal{E}_1 \times \dots \times \mathcal{E}_n$ of noise (exogeneous) variables $\epsilon_1, \dots, \epsilon_n$;
- a directed acyclic graph $\mathcal{G}(\mathcal{C})$, whose nodes are the causal variables and edges represent causal relations between the variables;
- causal mechanisms $F = \{f_1, \dots, f_n\}$ with $f_i : \mathcal{E}_i \times \prod_{j \in \text{pa}_i} \mathcal{Z}_j \rightarrow \mathcal{Z}_i$; and
- a probability measure $p_{\mathcal{E}}(\epsilon) = p_{\mathcal{E}_1}(\epsilon_1) p_{\mathcal{E}_2}(\epsilon_2) \dots p_{\mathcal{E}_n}(\epsilon_n)$ with full support that admits a continuous density.

Additionally, we assume that $\forall i, \forall z_{\text{pa}_i}, f_i(\cdot, z_{\text{pa}_i}) : \mathcal{E}_i \rightarrow \mathcal{Z}_i$ is a diffeomorphism.

We will need to reason about vectors being “equal up to permutation and elementwise reparameterizations”. We formalize this in the following definition:

Definition 5 (ψ -diagonal). *Let $\psi : [n] \rightarrow [n]$ be a bijection (that is, a permutation). Let $\varphi : \prod_{i=1}^n X_i \rightarrow \prod_{i=1}^n Y_i$ be a function between product spaces. Then φ is ψ -diagonal if there exist functions, called components, $\varphi_i : X_i \rightarrow Y_{\psi(i)}$ such that $\forall i, \forall x, \varphi(x_1, \dots, x_i, \dots, x_n)_{\psi(i)} = \varphi_i(x_i)$.*

This lets us define isomorphisms between SCMs:

Definition 6 (Isomorphism of SCMs). *Let $\mathcal{C} = \langle \mathcal{Z}, \mathcal{E}, F, p_{\mathcal{E}} \rangle$ and $\mathcal{C}' = \langle \mathcal{Z}', \mathcal{E}', F', p'_{\mathcal{E}} \rangle$ be SCMs. An isomorphism $\varphi : \mathcal{C} \rightarrow \mathcal{C}'$ consists of*

1. a graph isomorphism $\psi : \mathcal{G}(\mathcal{C}) \rightarrow \mathcal{G}(\mathcal{C}')$ that tells us how to identify corresponding variables in the two models and which preserves parents: $\text{pa}_{\psi(i)}^{\mathcal{C}'} = \psi(\text{pa}_i^{\mathcal{C}})$ and
2. ψ -diagonal diffeomorphisms for noise and endogenous variables that tell us how to reparameterize them $\varphi_{\mathcal{E}} : \mathcal{E} \rightarrow \mathcal{E}'$ and $\varphi_{\mathcal{Z}} : \mathcal{Z} \rightarrow \mathcal{Z}'$, where $\varphi_{\mathcal{E}}$ must be measure preserving $p_{\mathcal{E}'} = \varphi_{\mathcal{E}*}p_{\mathcal{E}}$. For notational simplicity, we will drop the subscript in $\varphi_{\mathcal{Z}}$ and use the symbol φ to refer both to the SCM isomorphism and the noise isomorphism.

The elementwise diffeomorphisms are required to make the following diagrams commute $\forall i, i' = \psi(i)$:

$$\begin{array}{ccc}
\mathcal{Z}_{\text{pa}_i} \times \mathcal{E}_i & \xrightarrow{(\varphi_{\text{pa}_i}, \varphi_{\mathcal{E}, i})} & \mathcal{Z}'_{\text{pa}'_i} \times \mathcal{E}'_i \\
\downarrow f_i & & \downarrow f'_i \\
\mathcal{Z}_i & \xrightarrow{\varphi_i} & \mathcal{Z}'_i
\end{array} \tag{5}$$

Intuitively, this says that if we apply a causal mechanism f_i and then reparameterize the causal variable i using φ_i , we get the same thing as first reparameterizing the parents and noise variable of variable i , and then applying the causal mechanism f'_i .

To reason about interventions, we equip SCMs with intervention distributions in the following definition.

Definition 7 (Intervention structural causal model (ISCM)). *An intervention structural causal model (ISCM) is a tuple $\mathcal{D} = \langle \mathcal{C}, \mathcal{I}, p_{\mathcal{I}} \rangle$ of*

1. *an acyclic SCM $\mathcal{C} = \langle \mathcal{Z}, \mathcal{E}, F, p_{\mathcal{E}} \rangle$ that admits a faithful distribution, meaning that conditional independence of causal variables z implies d -separation [24].*
2. *a set \mathcal{I} of interventions on \mathcal{C} , where each intervention $(I, (\tilde{f}_i)_{i \in I}) \in \mathcal{I}$ consist of*
 - (a) *a subset $I \subset \{1, \dots, n\}$ of the causal variables, called the intervention target set, and*
 - (b) *for each $i \in I$, a new causal mechanism $\tilde{f}_i : \mathcal{E}_i \rightarrow \mathcal{Z}_i$ which replaces the original mechanism and which does not depend on the parents.*

We define intervention set \mathcal{I} to be atomic if the number of targeted variables is one or zero.
3. *a probability measure $p_{\mathcal{I}}$ over \mathcal{I} .*

We can extend the notion of isomorphism from SCMs to ISCMs.

Definition 8 (Isomorphism of ISCMs). *Let $\mathcal{D} = \langle \mathcal{C}, \mathcal{I}, p_{\mathcal{I}} \rangle$ and $\mathcal{D}' = \langle \mathcal{C}', \mathcal{I}', p'_{\mathcal{I}'} \rangle$ be ISCMs. An ISCM isomorphism is an SCM isomorphism $\varphi : \mathcal{C} \rightarrow \mathcal{C}'$ with underlying graph isomorphism $\psi : \mathcal{G}(\mathcal{C}) \rightarrow \mathcal{G}(\mathcal{C}')$ and a ψ -diagonal diffeomorphism $\tilde{\varphi}_{\mathcal{E}} : \mathcal{E} \rightarrow \mathcal{E}'$ such that*

- *the graph isomorphism ψ induces a bijection of intervention sets*

$$\psi_{\mathcal{I}} : \mathcal{I} \rightarrow \mathcal{I}' : (I, (\tilde{f}_i)_{i \in I}) \mapsto (\psi(I), (\tilde{f}'_{i'})_{i' \in \psi(I)})$$

- *for each intervention $(I, (\tilde{f}_i)_{i \in I}) \in \mathcal{I}$, and each intervened on variable $i \in I$, the following diagram commutes:*

$$\begin{array}{ccc}
\mathcal{E}_i & \xrightarrow{\tilde{\varphi}_{\mathcal{E}, i}} & \mathcal{E}'_{\psi(i)} \\
\downarrow \tilde{f}_i & & \downarrow \tilde{f}'_{\psi(i)} \\
\mathcal{Z}_i & \xrightarrow{\varphi_i} & \mathcal{Z}'_{\psi(i)}
\end{array} \tag{6}$$

- *$\tilde{\varphi}_{\mathcal{E}}$ is measure preserving, i. e. $p_{\mathcal{E}'} = (\tilde{\varphi}_{\mathcal{E}})_* p_{\mathcal{E}}$.*
- *the bijection $\psi_{\mathcal{I}} : \mathcal{I} \rightarrow \mathcal{I}'$ preserves the distribution over interventions: $\psi_* p_{\mathcal{I}} = p'_{\mathcal{I}'}$.*

Latent Causal Models (LCMs), defined in Def. 1, add a map to the data space to an ILCM. We can lift ISCM isomorphisms to LCM isomorphisms by requiring that these decoders must respect the ISCM isomorphism.

Definition 9 (Isomorphism of LCMs). *Let $\mathcal{M} = \langle \mathcal{C}, \mathcal{X}, g, \mathcal{I}, p_{\mathcal{I}} \rangle$ and $\mathcal{M}' = \langle \mathcal{C}', \mathcal{X}, g', \mathcal{I}', p'_{\mathcal{I}'} \rangle$ be LCMs with identical observation space $\mathcal{X} = \mathcal{X}'$. An LCM isomorphism is an ISCM isomorphism $\varphi : \mathcal{D} \rightarrow \mathcal{D}'$ such that the decoders respect the SCM isomorphism, so this diagram must commute:*

$$\begin{array}{ccc}
\mathcal{Z} & \xrightarrow{\varphi} & \mathcal{Z}' \\
\searrow g & & \swarrow g' \\
& \mathcal{X} &
\end{array} \tag{7}$$

Remark 1. By defining objects and isomorphisms, we have defined a groupoid of SCMs, a groupoid of ISCMs and a groupoid of LCMs, as the isomorphisms are composed and inverted in an obvious way.

$$\begin{array}{ccc}
\epsilon, \tilde{\epsilon} & \xrightarrow{\varphi_{\mathcal{E}}, \tilde{\varphi}_{\mathcal{E}}} & \epsilon', \tilde{\epsilon}' \\
s, \tilde{s}_I \downarrow & & \downarrow s', \tilde{s}'_I \\
z, \tilde{z} & \xrightarrow{\varphi_{\mathcal{Z}}, \varphi_{\mathcal{Z}}} & z', \tilde{z}' \\
g, g \downarrow & & \downarrow g', g' \\
x, \tilde{x} & \xlongequal{\quad\quad\quad} & x, \tilde{x}
\end{array}$$

Figure 9: An illustration of the spaces and maps in our definitions and proof. When LCMs $\mathcal{M}, \mathcal{M}'$ are isomorphic, all squares in the diagram should commute. Additionally, all maps should preserve the weakly supervised distributions on the variables and all horizontal maps should be ψ -diagonal. Note that the latent variables (ϵ, z) can differ up to a diffeomorphism, but the x variables are actually observed, so must be identically equal. From that equality, the other horizontal maps are uniquely defined.

Definition 10 (Equivalence). We call two SCMs, ISCMs, or LCMs equivalent if an isomorphism exists between them.

Informally, two SCMs, ISCMs, or LCMs are equivalent if there is a ψ -diagonal map between their causal variables (i. e. the causal variables are equal up to permutation and elementwise diffeomorphisms), there is a ψ -diagonal map between their noise encodings, and all other structure (decoders, intervention sets, intervention distributions) is compatible with these reparameterizations.

Next, we define the solution function of an SCM or ISCM, which maps from noise variables to causal variables by repeatedly applying the causal mechanisms.

Definition 11 (Solution). Given an ISCM $\mathcal{D} = \langle \mathcal{C}, \mathcal{I}, p_{\mathcal{I}} \rangle$, the solution function $s : \mathcal{E} \rightarrow \mathcal{Z}$ is the unique function such that for all $i \in [n]$, the following diagram commutes [25]

$$\begin{array}{ccc}
& \mathcal{E} & \\
(s_{\text{pa}_i}, \text{id}_{\mathcal{E}_i}) \swarrow & & \searrow s_i \\
\mathcal{Z}_{\text{pa}_i} \times \mathcal{E}_i & \xrightarrow{f_i} & \mathcal{Z}_i
\end{array}$$

In equations, we have that $s(\epsilon)_i = f(\epsilon_i; s(\epsilon_{\text{pa}_i}))$. Similarly, intervention $(I, (\tilde{f}_i)_{i \in I}) \in \mathcal{I}$ yields a solution function $\tilde{s}_I : \mathcal{E} \rightarrow \mathcal{Z}$ with the modified causal mechanisms.

For example, with two variables with $z_1 \rightarrow z_2$, the solution is given by:

$$s : \mathcal{E} \rightarrow \mathcal{Z} : \begin{pmatrix} \epsilon_1 \\ \epsilon_2 \end{pmatrix} \mapsto \begin{pmatrix} z_1 \\ z_2 \end{pmatrix} = \begin{pmatrix} f_1(\epsilon_1) \\ f_2(\epsilon_2, f_1(\epsilon_1)) \end{pmatrix}.$$

Since we require causal mechanisms to be pointwise diffeomorphic, the solution function is a diffeomorphism as well.

Pushing the noise distribution of an SCM through the solution function finally gives us the (observable) distribution entailed by an SCM or ISCM. In an ISCM or LCM we can define several other (observational or interventional) distributions.

Definition 12 (Distributions). Given an LCM $\mathcal{M} = \langle \mathcal{C}, \mathcal{X}, g, \mathcal{I}, p_{\mathcal{I}} \rangle$, we have the following generative process:

$$\begin{aligned}
\epsilon &\sim p_{\mathcal{E}}, & z &= s(\epsilon), & x &= g(z), & e &= s^{-1}(z) \\
I &\sim p_{\mathcal{I}}, & \tilde{\epsilon} &\sim \tilde{p}_{\tilde{\mathcal{E}}}(\tilde{\epsilon} \mid \epsilon, I), & \tilde{z} &= \tilde{s}_I(\tilde{\epsilon}), & \tilde{x} &= g(\tilde{z}), & \tilde{e} &= s^{-1}(\tilde{z}).
\end{aligned} \quad (8)$$

where $p(\tilde{\epsilon}_i \mid \epsilon_i, i \in I) = p_{\mathcal{E}_i}(\tilde{\epsilon}_i)$ and $p(\tilde{\epsilon}_i \mid \epsilon_i, i \notin I) = \delta(\tilde{\epsilon}_i \mid \epsilon_i)$ is the Dirac measure.

Then we define the following weakly supervised distributions:

- The weakly supervised noise distribution with interventions: $p_{\mathcal{C}}^{\mathcal{E}, \mathcal{I}}(\epsilon, \tilde{\epsilon}, I)$.
- The weakly supervised causal distribution with interventions: $p_{\mathcal{C}}^{\mathcal{Z}, \mathcal{I}}(z, \tilde{z}, I)$.

- The weakly supervised observational distribution with interventions: $p_{\mathcal{M}}^{\mathcal{X}, \mathcal{I}}(x, \tilde{x}, I)$.

These distributions are given by appropriate pushforwards of the noise distributions through the transformations in Eq. (8).

By marginalizing over I , we get $p_C^{\mathcal{E}}, p_C^{\mathcal{Z}}, p_C^{\mathcal{e}}, p_{\mathcal{M}}^{\mathcal{X}}$ respectively.

The relationships between all the maps can be found in Fig. 9.

A.2 Identifiability proof

First, we prove two auxiliary lemmata.

Lemma 1. *Let $f : [0, 1] \rightarrow [0, 1]$ be differentiable and Lebesgue measure preserving. Then either $f(x) = x$ or $f(x) = 1 - x$.*

Proof. We follow the celebrated proof from Stack Exchange user zhw [35]. Let λ be the Lebesgue measure. Measure preservation means that for any measurable subset $U \subseteq [0, 1]$, $\lambda(U) = \lambda(f^{-1}(U))$.

First, note that f is surjective, because otherwise the image of f is a proper subinterval $[a, b] \subsetneq [0, 1]$ and $\lambda(f^{-1}([a, b])) = \lambda([0, 1]) = 1 > \lambda([a, b]) = b - a$, which contradicts measure-preservation.

Define the open ball $B(x, r) = \{y \in [0, 1] \mid |y - x| < r\}$. Suppose that $f'(0) = 0$ for some $x \in [0, 1]$. Then there exists an $r > 0$ such that $f(B(x, r)) \subseteq B(f(x), r/4)$, and thus $B(x, r) \subseteq f^{-1}(B(f(x), r/4))$. Therefore, $r \leq \lambda(B(x, r)) \leq \lambda(f^{-1}(B(f(x), r/4)))$, while $\lambda(B(f(x), r/4)) \leq 2 \cdot r/4 = r/2$, contradicting measure preservation. Hence $f'(x) \neq 0$ on $[0, 1]$.

By the Darboux theorem, f' is either strictly positive or strictly negative on the interval and thus f is either strictly increasing or decreasing and thus a bijection. Assume that it is strictly increasing, then $\forall x \in [0, 1]$, $x = \lambda([0, x]) = \lambda(f^{-1}(f([0, x]))) = \lambda(f([0, x])) = f(x) - f(0) = f(x)$. Similarly, if it is strictly decreasing, we find $f(x) = 1 - x$. \square

Lemma 2. *Let $A = C = \mathbb{R}$ and $B = \mathbb{R}^n$. Let $f : A \times B \rightarrow C$ be differentiable. Define differentiable measures p_A on A and p_C on C . Let $\forall b \in B$, $f(\cdot, b) : A \rightarrow C$ be measure-preserving. Then f is constant in B .*

Proof. Let $P_A : A \rightarrow [0, 1]$, $P_C : C \rightarrow [0, 1]$ be the diffeomorphic cumulative density functions. Then P_A^{-1} and P_C^{-1} are measure-preserving maps from the uniform distribution on $[0, 1]$. Now write $g : [0, 1] \times B \rightarrow [0, 1] : (z, b) \mapsto P_C(f(P_A^{-1}(z), b))$ such that this diagram of measure-preserving differentiable maps commutes:

$$\begin{array}{ccc}
 A & \xrightarrow{f(\cdot, b)} & C \\
 \searrow P_A & & \nearrow P_C^{-1} \\
 [0, 1] & \xrightarrow{g(\cdot, b)} & [0, 1]
 \end{array}$$

Then g is differentiable and $\forall b \in B$ measure-preserving $[0, 1] \rightarrow [0, 1]$. By the previous Lemma 1, the only differentiable measure-preserving functions $[0, 1] \rightarrow [0, 1]$ are id and $1 - \text{id}$. As g is continuous in B , it can not vary between id and $1 - \text{id}$ and thus g , and consequently f are constant in B . \square

We can interpret this lemma in terms of statistical independence. Starting from a product measure on $A \times B$, the requirements of the lemma correspond to $a \perp\!\!\!\perp b$ and $c \perp\!\!\!\perp b$. The lemma thus defines a sense in which for real-valued variables, statistical independence implies functional independence (the converse is always true).

Now in the remainder of this subsection, we prove the main theorem.

Theorem 1 (Identifiability of \mathbb{R} -valued LCMs from weak supervision). *Let $\mathcal{M} = \langle C, \mathcal{X}, g, \mathcal{I}, p_{\mathcal{I}} \rangle$ and $\mathcal{M}' = \langle C', \mathcal{X}', g', \mathcal{I}', p'_{\mathcal{I}'} \rangle$ be LCMs with the following properties:*

- The SCMs \mathcal{C} and \mathcal{C}' both consist of n real-valued endogeneous variables, i. e. $\mathcal{E}_i = \mathcal{Z}_i = \mathcal{Z}'_i = \mathcal{E}'_i = \mathbb{R}$.

- The intervention sets \mathcal{I} and \mathcal{I}' consist of the empty intervention and all atomic interventions, $\mathcal{I} = \{\emptyset, \{z_0\}, \dots, \{z_n\}\}$ and similar for \mathcal{I}' .
- The intervention distribution $p_{\mathcal{I}}$ and $p_{\mathcal{I}'}$ have full support.

Then the following two statements are equivalent:

1. The weakly supervised distributions entailed by the LCMs are equal, $p_{\mathcal{M}}(x, \tilde{x}) = p_{\mathcal{M}'}(x, \tilde{x})$.
2. The LCMs are equivalent, $\mathcal{M} \sim \mathcal{M}'$.

Proof. “(2) \Rightarrow (1)”: If the LCMs are equivalent, then the fact that $\varphi_{\mathcal{E}}$ and $\tilde{\varphi}_{\mathcal{E}}$ are measure preserving and that diagrams (5) and (6) commute, implies that $p_{\mathcal{C}'}^{\mathcal{Z}'} = (\varphi_{\mathcal{Z}}, \varphi_{\mathcal{Z}})_{*} p_{\mathcal{C}}^{\mathcal{Z}}$. Then because diagram (7) commutes, the weakly supervised distributions coincide, $p_{\mathcal{M}'}^{\mathcal{X}} = p_{\mathcal{M}}^{\mathcal{X}}$.

“(1) \Rightarrow (2)”: Conversely, if the weakly supervised distributions coincide, $p_{\mathcal{M}'}^{\mathcal{X}} = p_{\mathcal{M}}^{\mathcal{X}}$, the images of $g : \mathcal{Z} \rightarrow \mathcal{X}, g' : \mathcal{Z}' \rightarrow \mathcal{X}$ coincide,

$$\varphi = g'^{-1} \circ g : \mathcal{Z} \rightarrow \mathcal{Z}' \quad (9)$$

is a diffeomorphism, and φ preserves the weakly supervised distribution over causal variables: $p_{\mathcal{C}'}^{\mathcal{Z}'} = (\varphi, \varphi)_{*} p_{\mathcal{C}}^{\mathcal{Z}}$.

LCM equivalence then follows from showing that $\varphi : \mathcal{D} \rightarrow \mathcal{D}'$ is an ISCM isomorphism, where $\mathcal{D} = \langle \mathcal{C}, \mathcal{I}, p_{\mathcal{I}} \rangle$ and $\mathcal{D}' = \langle \mathcal{C}', \mathcal{I}', p_{\mathcal{I}'} \rangle$ be the ISCMs inherent to \mathcal{M} and \mathcal{M}' . We show this in the following steps:

1. For each intervention I in \mathcal{D} , there is a corresponding intervention I' in \mathcal{D}' , given by a permutation $\psi : [n] \rightarrow [n]$, such that φ preserves the interventional distribution.
2. The diffeomorphism φ is ψ -diagonal.
3. The permutation ψ preserved the ancestry structure of graphs $\mathcal{G}(\mathcal{C})$ and $\mathcal{G}(\mathcal{C}')$.
4. The diffeomorphism $\varphi_{\mathcal{E}} : \mathcal{E} \rightarrow \mathcal{E}$ of noise variables is ψ -diagonal.
5. The causal mechanisms are compatible with φ .

Step 1: Interventions preserved Remember that the diffeomorphism $\varphi : \mathcal{Z} \rightarrow \mathcal{Z}'$ is such that $p_{\mathcal{C}'}^{\mathcal{Z}'} = (\varphi, \varphi)_{*} p_{\mathcal{C}}^{\mathcal{Z}}$. For atomic interventions $I \neq J \in \mathcal{I}$, consider the intersection of the supports of the weakly supervised distribution for interventions on I and J : $U = \text{supp } p_{\mathcal{C}}^{\mathcal{Z}, \mathcal{I}}(z, \tilde{z} | I) \cap \text{supp } p_{\mathcal{C}}^{\mathcal{Z}, \mathcal{I}}(z, \tilde{z} | J) \subset \mathcal{Z} \times \mathcal{Z}$. Note that U has zero measure in $p_{\mathcal{C}}^{\mathcal{Z}, \mathcal{I}}(U | I) = p_{\mathcal{C}}^{\mathcal{Z}, \mathcal{I}}(U | J) = 0$. The distribution is thus a discrete mixture on (z, \tilde{z}) of non-overlapping distributions.

The diffeomorphism (φ, φ) must map between these mixtures. Thus there exists a bijection $\psi : \mathcal{I} \rightarrow \mathcal{I}'$, also inducing a permutation $\psi : [n] \rightarrow [n]$, such that

$$p_{\mathcal{C}'}^{\mathcal{Z}', \mathcal{I}'} = (\varphi, \varphi, \psi)_{*} p_{\mathcal{C}}^{\mathcal{Z}, \mathcal{I}}.$$

Step 2: φ is ψ -diagonal This measure preservation lets us define two equal distributions on $\mathcal{Z} \times \tilde{\mathcal{Z}}' \times \mathcal{I}$, namely $(\text{id}_{\mathcal{Z}}, \varphi, \text{id}_{\mathcal{I}})_{*} p_{\mathcal{C}}^{\mathcal{Z}, \mathcal{I}}$ and $(\varphi^{-1}, \text{id}_{\tilde{\mathcal{Z}}'}, \psi^{-1})_{*} p_{\mathcal{C}'}^{\mathcal{Z}', \mathcal{I}'}$. In particular, these must then have equal conditionals $p(\tilde{z}' | z, I)$. Thus, for any $U \subseteq \tilde{\mathcal{Z}}', z \in \mathcal{Z}, I \in \mathcal{I}$,

$$p_{\mathcal{C}'}^{\mathcal{Z}', \mathcal{I}'}(\tilde{z}' \in U | \varphi(z), \psi(I)) = p_{\mathcal{C}}^{\mathcal{Z}, \mathcal{I}}(\tilde{z} \in \varphi^{-1}(U) | z, I)$$

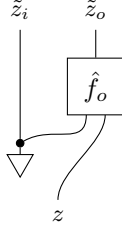
The conditional probability $p_{\mathcal{C}}^{\mathcal{Z}, \mathcal{I}}(\tilde{z} | z, I)$ can be interpreted as a stochastic map $\mathcal{Z} \rightarrow \tilde{\mathcal{Z}}$. The above relation can then be written as a commuting diagram of stochastic maps, $\forall I \in \mathcal{I}, I' = \psi(I)$:

$$\begin{array}{ccc} \mathcal{Z} & \xrightarrow{p_{\mathcal{C}}^{\mathcal{Z}, \mathcal{I}}(\tilde{z} | z, I)} & \tilde{\mathcal{Z}} \\ \downarrow \varphi & & \downarrow \varphi \\ \mathcal{Z}' & \xrightarrow{p_{\mathcal{C}'}^{\mathcal{Z}', \mathcal{I}'}(\tilde{z}' | z', I')} & \tilde{\mathcal{Z}}' \end{array} \quad (10)$$

where we treat $\varphi : \mathcal{Z} \rightarrow \mathcal{Z}'$ as a deterministic stochastic map.

For any variable $i \in [n]$, write the other nodes as $o = [n] \setminus \{i\}$. Let $I = \{i\}$. Then $p_{\mathcal{C}}^{\mathcal{Z}, \mathcal{I}}(\tilde{z} | z, I)$ can

be written as a string diagram of stochastic maps:



This string diagram represents a conditional probability distribution $p(\tilde{z}_i, \tilde{z}_o | z)$ and is read from the bottom to the top. String diagrams map formally to a generative process [36] and have been used previously in the context of causal models [37]. In this case, the diagram maps to:

$$\tilde{z}_i \sim p(\tilde{z}_i), \quad \tilde{z}_o = \hat{f}_o(\tilde{z}_i, z)$$

where $p(\tilde{z}_i)$ is the interventional distribution and the deterministic map $\hat{f}_o : \tilde{\mathcal{Z}}_i \times \mathcal{Z} \rightarrow \tilde{\mathcal{Z}}_o$ can be constructed from the inverse solution $s^{-1} : \mathcal{Z} \rightarrow \mathcal{E}$ and the causal mechanisms. Each box in a string diagram of stochastic maps denotes a stochastic map and each line to a measurable space. The triangle is the stochastic map $\star \rightarrow \tilde{\mathcal{Z}}_i$ (the star denoting the one-point space; maps from which correspond to probability distributions over the codomain). The \bullet represents copying a variable.

The above commuting diagram (10) can then be written as the equality of the following two string diagrams, where $\psi(I) = I' = \{i'\}, o' = [n] \setminus \{i'\}$. We write $\varphi : \mathcal{Z} \rightarrow \mathcal{Z}'$ as the pair $\varphi_{i'} : \mathcal{Z} \rightarrow \mathcal{Z}'_{i'}, \varphi_{o'} : \mathcal{Z} \rightarrow \mathcal{Z}'_{o'}$ obtained by projecting the output of φ to the partition $\mathcal{Z}' = \mathcal{Z}'_{i'} \times \mathcal{Z}'_{o'}$:

(11)

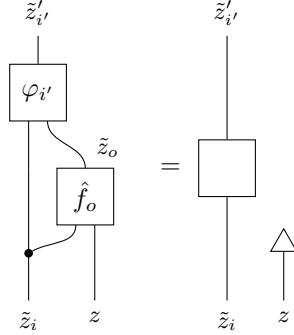
This should be read as the equality of the two conditional probability distributions $p(\tilde{z}'_{i'}, \tilde{z}'_{o'} | z)$ generated in the following way:

$$\begin{aligned} \text{Left: } & \tilde{z}_i \sim p(\tilde{z}_i), \quad \tilde{z}_o = \hat{f}_o(\tilde{z}_i, z), \quad \tilde{z}'_{i'} = \varphi(\tilde{z}_i, \tilde{z}_o)_{i'}, \quad \tilde{z}'_{o'} = \varphi(\tilde{z}_i, \tilde{z}_o)_{o'}. \\ \text{Right: } & z' = \varphi(z), \quad \tilde{z}'_{i'} \sim p'(\tilde{z}'_{i'}), \quad \tilde{z}'_{o'} = \hat{f}'_{o'}(\tilde{z}'_{i'}, z'). \end{aligned}$$

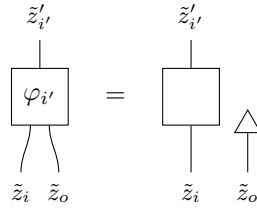
The string diagram equality (11) implies equality when we disregard outputs $\mathcal{Z}'_{o'}$:

where the upwards pointing triangle represents discarding a variable.

Using Lemma 2, and the fact that $\tilde{\mathcal{Z}}_i = \tilde{\mathcal{Z}}_{i'} = \mathbb{R}$, the composed differentiable function $\tilde{\mathcal{Z}}_i \times \mathcal{Z} \rightarrow \tilde{\mathcal{Z}}_{i'}$ is constant in \mathcal{Z} . Thus we have a deterministic function $\tilde{\mathcal{Z}}_i \rightarrow \tilde{\mathcal{Z}}_{i'}$ such that:

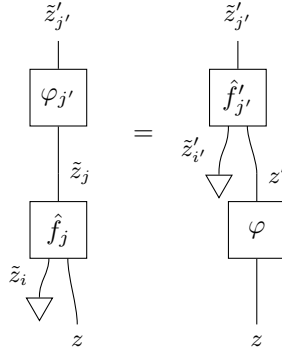


The deterministic function $\tilde{\mathcal{Z}}_i \times \mathcal{Z} \rightarrow \tilde{\mathcal{Z}}_i \times \tilde{\mathcal{Z}}_o$ is surjective and both the left- and right-hand side can be seen as first applying this function (though the output is discarded on the right hand side), which implies there exists a function $\tilde{\mathcal{Z}}_i \rightarrow \tilde{\mathcal{Z}}_{i'}$ such that



In words, the function $\varphi_{i'} : \mathcal{Z}_i \times \mathcal{Z}_o \rightarrow \mathcal{Z}'_{i'}$ is constant in \mathcal{Z}_o . This holds for all i and thus φ is ψ -diagonal.

Step 3: Ancestry preserved Let $i \neq j \in [n]$, $i' = \psi(i)$, $j' = \psi(j)$, and $I = \{i\}$. Writing φ as ψ -diagonal, the commuting diagram (10) for the j' component of \tilde{z}' , can be written as the following string diagram:



The left hand side is a deterministic map $\mathcal{Z} \rightarrow \tilde{\mathcal{Z}}'_{j'}$, if and only if \hat{f}_j is constant in $\tilde{\mathcal{Z}}_i$ which by faithfulness is the case if and only if $i \notin \mathbf{anc}_j$. The same holds on the right hand side, so $\forall i \neq j \in [n]$, $i \in \mathbf{anc}_j^C \iff \psi(i) \in \mathbf{anc}_{\psi(j)}^C$.

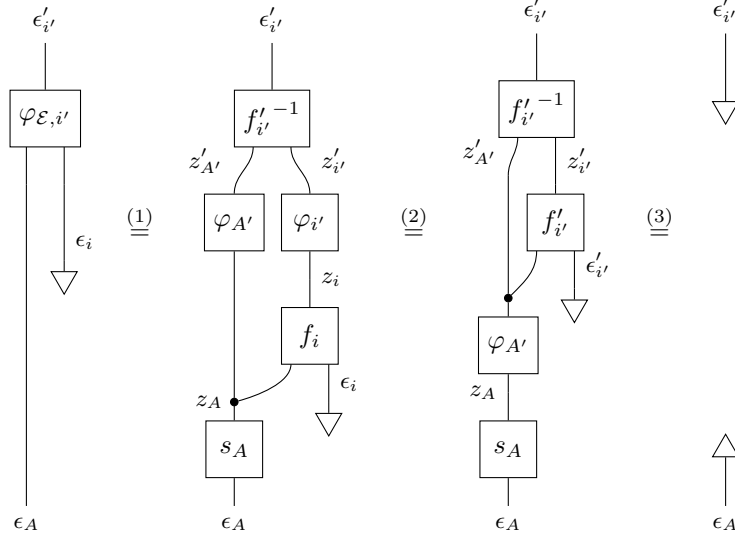
Step 4: Noise map diagonal Define $\varphi_{\mathcal{E}} = s'^{-1} \circ \varphi \circ s : \mathcal{E} \rightarrow \mathcal{E}'$. Note that $\varphi_{\mathcal{E}}(\epsilon)_{i'}$ only depends on ϵ_i and $\epsilon_{\mathbf{anc}_i}$, because $s(\epsilon)_{\mathbf{anc}_i, i}$ and $s'^{-1}(z')_{i'}$ only depend on ancestors, φ is ψ -diagonal and ψ preserves ancestry.

The map φ is measure-preserving. Thus $\forall i$ and writing $A = \mathbf{anc}_i$, the conditional $p(z_i | z_A) = p(z_i | z_{\mathbf{pa}_i})$, interpreted as a stochastic map, is preserved by φ . We can express this as another

commuting diagram, in which the two paths from \mathcal{E}_A to $\mathcal{E}'_{i'}$ must be equal:

$$\begin{array}{ccccc} \mathcal{E}_A & \xrightarrow{s_A} & \mathcal{Z}_A & \xrightarrow{p(z_i|z_{\text{pa}_i})} & \mathcal{Z}_{A,i} \\ & & \varphi_A \downarrow & & \downarrow \varphi_{A,i} \\ & & \mathcal{Z}'_{A'} & \xrightarrow{p(z'_{i'}|z'_{\text{pa}_{i'}})} & \mathcal{Z}'_{A',i'} \xrightarrow{f'_{i'}^{-1}} & \mathcal{E}'_{i'} \end{array}$$

where $f'_{i'}^{-1}(z') = f(z'_{\text{pa}_{i'}}, \cdot)^{-1}(z')$. Then we have:



where the first equality follows from the definition of $\varphi_{\mathcal{E},i'}$, the second equality from the commuting diagram above and the third equality from the fact that $f'_{i'}$ and $f'_{i'}^{-1}$ cancel. Then, again using Lemma 2, the map on the left hand side must be constant in ϵ_A . The noise encoding is thus also ψ -diagonal.

Step 5: Equivalence Consider for a variable i and with $i' = \psi(i)$ the following commuting diagram of deterministic maps. Note that we write the causal mechanism f_i as a function of all ancestors, not just the parents, so it is constant in the non-parents. Because of faithfulness, it is non-constant in the parents. Since ψ preserves ancestors, $f'_{i'}$ is well-typed.

$$\begin{array}{ccc} \mathcal{E} & \xrightarrow{\varphi_{\mathcal{E}}} & \mathcal{E}' \\ \downarrow (s_{\text{anc}_i}, \text{id}_{\mathcal{E}_i}) & & \downarrow (s'_{\text{anc}_{i'}}, \text{id}_{\mathcal{E}'_{i'}}) \\ \mathcal{Z}_{\text{anc}_i} \times \mathcal{E}_i & \xrightarrow{(\varphi_{\mathcal{Z},\text{anc}_i}, \varphi_{\mathcal{E},i})} & \mathcal{Z}'_{\text{anc}_{i'}} \times \mathcal{E}'_{i'} \\ \downarrow f_i & & \downarrow f'_{i'} \\ \mathcal{Z}_i & \xrightarrow{\varphi_{\mathcal{Z},i}} & \mathcal{Z}'_{i'} \end{array}$$

The composition of the left vertical maps is equal to s_i , the composition of the right vertical maps to $s'_{i'}$. Therefore and because of the definition of $\varphi_{\mathcal{E}}$, the outer and the top square commute. Then, because $(s_{\text{anc}_i}, \text{id}_{\mathcal{E}_i})$ is surjective, the bottom square also commutes [38, Lemma 1.6.21].

Then for $z_j \in \text{anc}_i$, we have that

$$z_j \in \text{pa}_i^{\mathcal{C}} \iff f_i \text{ not constant in } z_j \iff f'_{i'} \text{ not constant in } z'_{j'} \iff z'_{j'} \in \text{pa}_{i'}^{\mathcal{C}'}$$

And thus ψ not only preserves ancestry, but also parenthood and is thus a graph isomorphism $\psi : \mathcal{G}(\mathcal{C}) \rightarrow \mathcal{G}(\mathcal{C}')$. Diagram (5) commutes, and we have established an SCM isomorphism $\varphi : \mathcal{C} \rightarrow \mathcal{C}'$.

To have this also be an ISCM isomorphism, we need diagram (6) to commute and the distribution

over interventions to be preserved. For the first, use the fact that all maps in (6) are isomorphisms to simply define $\tilde{\varphi}_\mathcal{E}$ so that the diagram commutes. The second follows directly from the assumptions. Hence $\varphi : \mathcal{D} \rightarrow \mathcal{D}'$ is an ISCM isomorphism, $\mathcal{D} \sim \mathcal{D}'$, and—together with the arguments in the beginning of this proof—finally $\mathcal{M} \sim \mathcal{M}'$. \square

B Limitations & generalization

Our identifiability result relies on a few assumptions. Here we discuss some key requirements of Thm. 1 and whether they can be relaxed.

Diffeomorphic causal mechanisms In Def. 4, we require causal mechanisms to be pointwise diffeomorphisms from noise variables to causal variables. Under some mild smoothness assumptions, any SCM can be brought into this form by elementwise redefinitions of the variables, without affecting the observational or interventional distributions. However, such a redefinition may change counterfactual / weakly supervised distributions.

All interventions observed To guarantee identifiability, we require that the intervention distribution has support for any atomic intervention: datasets need to contain data pairs generated from interventions on any causal variable. However, in many systems not all variables can be intervened upon, for instance because some variables are fundamentally immutable or for safety reasons. In that case, the LCM may not be fully identifiable, but there may still be partial identifiability. Interventions on child variables, for instance, can guarantee the identifiability of the parents [14]. We leave a precise characterization of the equivalence classes under such partial weak supervision for future work.

Perfect interventions Our proof of Thm. 1 requires perfect interventions, i. e. that intervened-upon mechanisms do not depend on any causal variables. This is arguably the biggest mismatch between our assumptions and many real-world systems.

If we try to generalize this assumption and allow the intervention mechanisms to depend on the parent variables, identifiability is lost. A simple counterexample is the following.

Example 1 (Non-identifiable ISMCs under imperfect interventions). *Consider two inequivalent ISMCs $\mathcal{D}, \mathcal{D}'$, each with two variables and graph $z_1 \rightarrow z_2$. Let the mechanisms be equal, except that $f'_2(\epsilon_2; z_1) = f_2(\epsilon_2; z_1) + z_1$ and $\tilde{f}'_2(\tilde{\epsilon}_2; z_1) = \tilde{f}_2(\tilde{\epsilon}_2; z_1) + z_1$. Then it is easy to see that a ϕ that is the identity on the first variable and on the second variable is $\phi_2(z_1, z_2) = z_1 + z_2$, preserves the weakly supervised distribution, but is not an ISCM isomorphism.*

Diffeomorphic decoder Definition 1 and Thm. 1 assume that the map from causal variables to observed data is given by a deterministic, diffeomorphic decoder. However, our practical implementation in a VAE uses a stochastic decoder and allows for noisy data. Our experiments provide empirical evidence for identifiability in this setting. We believe that it may be possible to extend Thm. 1 to stochastic decoders, similarly to Khemakhem et al. [8]. We plan to study this extension in future work.

Independent of whether the decoder is deterministic or stochastic, however, is the requirement that the value of all causal variables need to be reflected in the observed low-level data. Our approach (and as far as we are aware all other methods for causal representation learning) is not able to detect causal variables that do not directly influence the low-level data. Latent confounders, present in many real-world problems, provide an as-of-now unsolved hurdle to causal representation learning.

Real-valued causal variables Theorem 1 assumes real-valued causal and noise variables, $\mathcal{Z}_i = \mathcal{E}_i = \mathbb{R}$. We can easily extend this to intervals $(a, b) \in \mathbb{R}$, as these are isomorphic to \mathbb{R} . However, the extension to arbitrary continuous spaces or \mathbb{R}^n is not straightforward. The main reason is that our proof relies on Lemma 2, which does not generalize.

Let us provide a counterexample for identifiability with circle S^1 -valued causal variables.

Example 2 (S^1 -valued non-identifiable LCMs). *Consider an LCM $\mathcal{M} = \langle \mathcal{C}, \mathcal{X}, g, \mathcal{I}, p_{\mathcal{I}} \rangle$ with the following components:*

- *The SCM \mathcal{C} consists of two circle-valued variables $z_1, z_2 \in S^1$ with noise variables $\epsilon_1, \epsilon_2 \in S^1$. We parameterize S^1 as $[0, 2\pi)$ with addition defined modulo 2π .*

- The causal graph is $z_1 \rightarrow z_2$.
- The causal mechanisms are $f_1(\epsilon_1) = \epsilon_1$ and $f_2(\epsilon_2; z_1) = \epsilon_2 + z_1$.
- The solution function is $s(\epsilon_1, \epsilon_2) = (\epsilon_1, \epsilon_2 + \epsilon_1)$.
- The noise variables are distributed as $\epsilon_1 \sim \mathcal{U}$, uniformly, and $\epsilon_2 \sim q$, which we require to not be invariant under translations (so in particular not uniform). For example, one can take the von Mises distribution $\log q(\epsilon_2) = \cos(\epsilon_2) + \text{const}$.
- The observation space is \mathcal{X} and the decoder $g : S^1 \times S^1 \rightarrow \mathcal{X}$ is diffeomorphic.
- The intervention set \mathcal{I} consists of the empty intervention, atomic interventions on z_1 with $\tilde{z}_1 \sim \mathcal{U}$, and atomic interventions on z_2 with $\tilde{z}_2 \sim \mathcal{U}$. Each of these interventions has probability $\frac{1}{3}$ in $p_{\mathcal{I}}$.

Note that the SCM is faithful, as $z_1 \not\perp\!\!\!\perp z_2$ in the observational distribution, because q is not translationally invariant. The LCM entails the weakly supervised causal distribution

$$p_{\mathcal{C}}^{\tilde{\mathcal{Z}}}(z, \tilde{z}) = \mathcal{U}(z_1) q(z_2 - z_1) \left[\frac{1}{3} \delta(\tilde{z}_1 - z_1) \delta(\tilde{z}_2 - z_2) + \frac{1}{3} \mathcal{U}(\tilde{z}_1) \delta(\tilde{z}_2 - z_2 - \tilde{z}_1 + z_1) + \frac{1}{3} \delta(\tilde{z}_1 - z_1) \mathcal{U}(\tilde{z}_2) \right] \quad (12)$$

with Dirac delta δ . The weakly supervised data distribution is then given by $p_{\mathcal{M}}^{\mathcal{X}} = (g_*, g_*)p_{\mathcal{C}}^{\tilde{\mathcal{Z}}}$.

Now consider a second LCM $\mathcal{M}' = \langle \mathcal{C}', \mathcal{X}, g', \mathcal{I}', p_{\mathcal{I}'}' \rangle$:

- The SCM \mathcal{C}' consists of two circle-valued variables $z'_1, z'_2 \in S^1$ with noise variables $\epsilon'_1, \epsilon'_2 \in S^1$.
- The causal graph is trivial and the causal mechanisms are given by the identity, $f'_i(\epsilon'_i) = \epsilon'_i$.
- The noise variables are distributed as $\epsilon'_1 \sim \mathcal{U}$ and $\epsilon'_2 \sim q$.
- The observation space is \mathcal{X} and the decoder $g' : S^1 \times S^1 \rightarrow \mathcal{X}$ is given by the diffeomorphism $g'(z') = g \circ s(z')$, where s is the solution function of \mathcal{C} .
- The intervention set \mathcal{I}' consists of empty interventions, atomic interventions on z'_1 with $\tilde{z}'_1 \sim \mathcal{U}$, and atomic interventions on z'_2 with $\tilde{z}'_2 \sim \mathcal{U}$. Each of these interventions has probability $\frac{1}{3}$ in $p_{\mathcal{I}'}'$.

We find a weakly supervised causal distribution

$$p_{\mathcal{C}'}^{\tilde{\mathcal{Z}}'}(z', \tilde{z}') = \mathcal{U}(z'_1) q(z'_2) \left[\frac{1}{3} \delta(\tilde{z}'_1 - z'_1) \delta(\tilde{z}'_2 - z'_2) + \frac{1}{3} \mathcal{U}(\tilde{z}'_1) \delta(\tilde{z}'_2 - z'_2) + \frac{1}{3} \delta(\tilde{z}'_1 - z'_1) \mathcal{U}(\tilde{z}'_2) \right]. \quad (13)$$

Clearly, two LCMs are not equivalent, because their graphs are non-isomorphic. Yet, if we define

$$\varphi : \mathcal{Z} \rightarrow \mathcal{Z}' : (z_1, z_2) \mapsto (z_1, z_2 - z_1)$$

then the weakly supervised distribution of the causal variables is preserved:

$$\begin{aligned} ((\varphi, \varphi)_* p_{\mathcal{C}}^{\tilde{\mathcal{Z}}})(z', \tilde{z}') &= p_{\mathcal{C}'}^{\tilde{\mathcal{Z}}'}((z'_1, z'_2 + z'_1), (\tilde{z}'_1, \tilde{z}'_2 + \tilde{z}'_1)) \\ &= \mathcal{U}(z'_1) q(z'_2 + z'_1 - z'_1) \left[\frac{1}{3} \delta(\tilde{z}'_1 - z'_1) \delta(\tilde{z}'_2 + \tilde{z}'_1 - (z'_2 + z'_1)) + \frac{1}{3} \mathcal{U}(\tilde{z}'_1) \delta(\tilde{z}'_2 + \tilde{z}'_1 - (z'_2 + z'_1) - \tilde{z}'_1 + z'_1) + \frac{1}{3} \delta(\tilde{z}'_1 - z'_1) \mathcal{U}(\tilde{z}'_2 + \tilde{z}'_1) \right] \\ &= \mathcal{U}(z'_1) q(z'_2) \left[\frac{1}{3} \delta(\tilde{z}'_1 - z'_1) \delta(\tilde{z}'_2 - z'_2) + \frac{1}{3} \mathcal{U}(\tilde{z}'_1) \delta(\tilde{z}'_2 - z'_2) + \frac{1}{3} \delta(\tilde{z}'_1 - z'_1) \mathcal{U}(\tilde{z}'_2) \right] \\ &= p_{\mathcal{C}'}^{\tilde{\mathcal{Z}}'}(z', \tilde{z}') \end{aligned}$$

where we use that the density \mathcal{U} is constant. Also, because $\varphi = s^{-1}$ and $g'(z') = g \circ s(z')$, we have that $p_{\mathcal{M}}^{\mathcal{X}} = p_{\mathcal{M}'}^{\mathcal{X}}$.

So these two models with their non-isomorphic graph structures have identical weakly-supervised distributions on the observables x, \tilde{x} . They therefore provide a counter-example for a straightforward generalization of Thm. 1 to causal variables with arbitrary continuous domains.

The key issue here is that the interventional distribution on \tilde{z}_2 has many symmetries or automorphisms: diffeomorphic maps $\mathcal{Z}_2 \rightarrow \mathcal{Z}_2$ that preserve $p(\tilde{z}_2)$ — in this case these are the cyclic translations. In general, for any causal model \mathcal{D} with two variables $z_1 \rightarrow z_2$, we can construct a map $\phi(z_1, z_2) = (z_1, \Gamma(z_1)(z_2))$ where for all z_1 , $\Gamma(z_1) : \mathcal{Z}_2 \rightarrow \mathcal{Z}_2$ is a differentiable map from \mathcal{Z}_1 to a diffeomorphism on \mathcal{Z}_2 that preserves the interventional distribution $p(\tilde{z}_2)$. This map ϕ preserves the weakly supervised distribution from \mathcal{D} to a unique model \mathcal{D}' , whose causal mechanisms are: $f'_1(\epsilon_1) = f_1(\epsilon_1)$ and $f'_2(z_1, \epsilon_1) = \Gamma(z_1)(f_2(z_1, \epsilon_2))$. However, ϕ is only an ISCM morphism if it is also diagonal, and thus Γ must be constant in z_1 .

For the \mathbb{R} -valued variables of the main paper, any smooth distribution on \mathbb{R} has exactly two automorphisms, related to the automorphisms of the univariate Gaussian distribution $x \mapsto x$ and $x \mapsto -x$. Γ can not smoothly switch between these and thus must be constant, making ϕ diagonal and an ISCM morphism. However, any multi-dimensional distribution has many automorphisms. One class of these is related to the orthogonal transformations of a standard multivariate Gaussian. Another, much larger, class is related to the flows generated by divergence-free vector fields on the unit ball. Γ can smoothly choose different such automorphisms for different values of z_1 , making ϕ not diagonal and thus not an ISCM morphism. In conclusion, this smooth space of automorphisms make the multivariate case unidentifiable from weak supervision.

C Implicit latent causal models

C.1 Behaviour of noise encodings under interventions

We first prove a key property of ISCMs, which motivate the construction of ILCMs:

Lemma 3. *Let $\mathcal{D} = \langle \mathcal{C}, \mathcal{I}, p_{\mathcal{I}} \rangle$ be an ISCM with n real-valued causal variables. Sample from the weakly-supervised distribution over noise encodings $(e, \tilde{e}) \sim p(e, \tilde{e}|I)$. Then $\forall i \notin I$, almost surely $e_i = \tilde{e}_i$.*

Proof. First, note that $z = s(\epsilon)$ and $e = s^{-1}(z)$, so $\epsilon = e$. If $i \notin I$, then the unintervened noise equals the intervened noise $\tilde{\epsilon}_i = \epsilon_i$, so

$$\begin{aligned} \tilde{e}_i &= s^{-1}(\tilde{z})_i \\ &= f_i(\cdot, \tilde{z}_{\mathbf{pa}_i})^{-1}(\tilde{z}_i) \\ &= f_i(\cdot, \tilde{z}_{\mathbf{pa}_i})^{-1}(f_i(\tilde{\epsilon}_i, \tilde{z}_{\mathbf{pa}_i})) \\ &= \tilde{\epsilon}_i = \epsilon_i = e_i \end{aligned} \quad \square$$

C.2 Model specification

An implicit latent causal model for a system of n causal variables consists of the following components:

- a Gaussian noise encoder $q(e|x)$ with mean $\mu_e(x)$ and standard deviation $\sigma_e(x)$ implemented as neural networks;
- a Gaussian noise decoder $p(x|e)$ with mean $\mu_x(e)$ implemented as neural network and fixed, constant standard deviation;
- an intervention encoder $q(I|x, \tilde{x})$ defined as

$$\log q(i \in I|x, \tilde{x}) = \frac{1}{Z} \left(a + b |\mu_e(x)_i - \mu_e(\tilde{x})_i| + c |\mu_e(x)_i - \mu_e(\tilde{x})_i|^2 \right),$$

where $a < 0$ and $b, c > 0$ are learnable parameters and where the normalization constant Z is defined such that $\sum_I q(i \in I|x, \tilde{x}) = 1$;

- solution functions $s_i(e_i; e_{\setminus i})$ for $i = 1, \dots, n$ implemented as invertible affine transformations, where the offset and slope are functions of $e_{\setminus i}$ implemented with neural networks;
- noise priors $p_i(e_i)$, which we choose to be standard Gaussian;

- an post-intervention causal-variable prior $\tilde{\pi}(\tilde{z}_i)$, which we choose to be standard Gaussian; and
- an intervention-target prior $p(I)$, which we choose to be uniform.

Encoding a data pair (x, \tilde{x}) during training consists of the following steps:

$$\begin{aligned}
I &\sim q(I|x, \tilde{x}) \\
e_{\text{preliminary}} &\sim q(e|x) & \tilde{e}_{\text{preliminary}} &\sim q(\tilde{e}_{\text{preliminary}}|\tilde{x}) \\
\forall i, \lambda_i &\sim \text{Uniform}(0, 1) & e_{\text{average } i} &= \lambda_i e_{\text{preliminary } i} + (1 - \lambda_i) \tilde{e}_{\text{preliminary } i} \\
e_i &= \begin{cases} e_{\text{preliminary } i} & i \in I \\ e_{\text{average } i} & i \notin I \end{cases} & \tilde{e}_i &= \begin{cases} \tilde{e}_{\text{preliminary } i} & i \in I \\ e_{\text{average } i} & i \notin I \end{cases}. \tag{14}
\end{aligned}$$

In the first line, we encode to an intervention target (either by sampling or by enumerating all possibilities and summing up the corresponding loss terms). In the second line, the data is encoded to the noise-encoding space. The third and fourth line project these noise encodings such that for those components e_i that are not intervened upon, $i \notin I$, we have that the pre-intervention noise encoding and post-intervention noise encoding are equal, $e_i = \tilde{e}_i$. This makes sure that the latents are consistent with the weakly supervised structure, and punishes deviations from this structure through the reconstruction error (likelihood). We use the symbol $e, \tilde{e} \sim q(e, \tilde{e}|x, \tilde{x}, I)$ to refer to the second to last line together.

The prior is given by

$$p(e, \tilde{e}_I, I) = p(I) \prod_i p_i(e_i) \prod_{i \in I} p(\tilde{e}_i|e)$$

with, for $i \in I$,

$$p(\tilde{e}_i|e) = \tilde{p}(s_i(\tilde{e}_i|e_{\setminus i})) \left| \frac{\partial \bar{s}_i(\tilde{e}_i; e_{\setminus i})}{\partial \tilde{e}_i} \right|. \tag{15}$$

C.3 Training

Loss We train ILCMs by minimizing the β -VAE loss

$$\begin{aligned}
\mathcal{L}_{\text{ILCM}} &= \mathbb{E}_{x, \tilde{x}} \mathbb{E}_{I \sim q(I|x, \tilde{x})} \mathbb{E}_{e, \tilde{e} \sim q(e, \tilde{e}|x, \tilde{x}, I)} \left[\log p(x|e) + \log p(\tilde{x}|\tilde{e}) \right. \\
&\quad \left. + \beta \left\{ \log p(e, \tilde{e}_I, I) - \log q(I|x, \tilde{x}) - \log q(e, \tilde{e}_I|x, \tilde{x}, I) \right\} \right],
\end{aligned}$$

where β is a hyperparameter.

Two additional loss terms are used as regularizers during training. The first is a plain reconstruction error (or log likelihood term) that does not use the projections given in Eq. (14) to encourage consistency between the noise encoder and noise decoder:

$$\mathcal{L}_{\text{reco}} = \mathbb{E}_{x, \tilde{x}} \mathbb{E}_{e \sim q(e|x)} \mathbb{E}_{\tilde{e} \sim q(\tilde{e}|\tilde{x})} \left[\log p(x|e) + \log p(\tilde{x}|\tilde{e}) \right].$$

Throughout training, we also add the negative entropy of the batch-aggregate intervention posterior $q_I^{\text{batch}}(I) = \mathbb{E}_{x, \tilde{x} \in \text{batch}} [q(I|x, \tilde{x})]$:

$$\mathcal{L}_{\text{entropy}} = \mathbb{E}_{\text{batches}} \left[- \sum_I q_I^{\text{batch}}(I) \log q_I^{\text{batch}}(I) \right].$$

This helps avoid a collapse of the latent space to a lower-dimensional subspace. The overall loss is then given by

$$\mathcal{L} = \mathcal{L}_{\text{ILCM}} + \alpha \mathcal{L}_{\text{reco}} + \gamma \mathcal{L}_{\text{entropy}} \tag{16}$$

with hyperparameters $\alpha, \gamma \geq 0$.

Algorithm 1 Schematic ILCM training.

Require: Training data $p_{\text{data}}(x, \tilde{x})$

Require: ILCM with encoder $q(e, \tilde{e}, I|x, \tilde{x})$, decoder $p(x|e)$, solution functions $s_i(e_i; e_{\setminus i})$.

Require: Optimizer

Require: Loss weights α, β , optimizer hyperparameters, ILCM initialization

- 1: Randomly initialize ILCM
 - 2: **while** not converged **do**
 - 3: Sample data batch $x, \tilde{x} \sim p_{\text{data}}(x, \tilde{x})$
 - 4: Encode $e \sim q^{\text{phase 1}}(x), \tilde{e} \sim q^{\text{phase 1}}(\tilde{x})$
 - 5: Compute loss $L \leftarrow \mathcal{L}^{\text{phase 1}}(x, \tilde{x})$ (Eq. (17))
 - 6: Train ILCM on L with optimizer
 - 7: **end while**
 - 8: **while** not converged **do**
 - 9: Sample data batch $x, \tilde{x} \sim p_{\text{data}}(x, \tilde{x})$
 - 10: Encode $e, \tilde{e}, I \sim q(e, \tilde{e}, I|x, \tilde{x})$ (Eq. (14))
 - 11: Compute loss $L \leftarrow \mathcal{L}^{\text{phase 2}}(x, \tilde{x})$ (Eq. (18))
 - 12: Train ILCM on L with optimizer
 - 13: **end while**
 - 14: Freeze convolutional layers in $q(e, \tilde{e}, I|x, \tilde{x})$
 - 15: **while** not converged **do**
 - 16: Sample data batch $x, \tilde{x} \sim p_{\text{data}}(x, \tilde{x})$
 - 17: Encode $e, \tilde{e}, I \sim q(e, \tilde{e}, I|x, \tilde{x})$ (Eq. (14))
 - 18: Compute loss $L \leftarrow \mathcal{L}(x, \tilde{x})$ (Eq. (16))
 - 19: Train ILCM on L with optimizer
 - 20: **end while**
 - 21: Determine top. order $o \leftarrow \text{TopoOrderHeuristic}(\text{ILCM}, p_{\text{data}}(x, \tilde{x}))$ (described in Sec. C.5)
 - 22: Modify s_i to only depend on $s_i(e_i; e_{\text{anc}_i})$ according to o
 - 23: **while** not converged **do**
 - 24: Sample data batch $x, \tilde{x} \sim p_{\text{data}}(x, \tilde{x})$
 - 25: Encode $e, \tilde{e}, I \sim q^{\text{phase 4}}(e, \tilde{e}, I|x, \tilde{x})$ (Eq. (20))
 - 26: Compute loss $L \leftarrow \mathcal{L}(x, \tilde{x})$ (Eq. (16))
 - 27: Train ILCM on L with optimizer
 - 28: **end while**
-

Training phases We train ILCM models in four phases:

1. We begin with a short pre-training phase, in which the noise encoder and noise decoder are trained on a plain β -VAE loss with a standard Gaussian prior,

$$\begin{aligned} \mathcal{L}^{\text{phase 1}} = \mathbb{E}_{x, \tilde{x}} \mathbb{E}_{e, \tilde{e} \sim q(e|x)q(\tilde{e}|\tilde{x})} & \left[\log p(x|e) + \log p(\tilde{x}|\tilde{e}) \right. \\ & \left. + \beta \left\{ \log \mathcal{N}(e) + \log \mathcal{N}(\tilde{e}) - \log q(e|x) - \log q(\tilde{e}|\tilde{x}) \right\} \right]. \quad (17) \end{aligned}$$

This provides a good starting point for the remainder of the training, in which the encoders and decoders have already learned some patterns in the data space.

2. Next, we train the noise encoder, noise decoder, and intervention encoder. In this phase we do not yet use the neural solution functions and instead model $p(\tilde{e}_i|e)$ with a uniform probability density. Ignoring irrelevant constants, the total loss is given by

$$\begin{aligned} \mathcal{L}^{\text{phase 2}} = \mathbb{E}_{x, \tilde{x}} \mathbb{E}_{I \sim q(I|x, \tilde{x})} \mathbb{E}_{e, \tilde{e} \sim q(e, \tilde{e}|x, \tilde{x}, I)} & \left[\log p(x|e) + \log p(\tilde{x}|\tilde{e}) + \beta \left\{ \log p(I) \right. \right. \\ & \left. \left. + \sum_i \log p_i(e_i) - \log q(I|x, \tilde{x}) - \log q(e, \tilde{e}|x, \tilde{x}, I) \right\} \right] + \alpha \mathcal{L}_{\text{reco}} + \gamma \mathcal{L}_{\text{entropy}}. \quad (18) \end{aligned}$$

This avoids harmful feedback from the randomly initialized solution functions influencing the training of the encoder and decoders, stabilizing the learning of good latent representations.

3. We then “switch on” the solution functions and model the intervention targets with the density $p(\tilde{e}_i|e)$ as given above and train on the combined loss \mathcal{L} .

On image datasets, we freeze the convolutional layers in the encoder in this stage and only continue training the final layers of the encoder together with the solution functions.

4. For a final fine-tuning phase, we change the setup in two more ways. First, we analyze the learned solution functions to infer the most likely topological order. For this we use the step 1 of the heuristic algorithm for graph inference, which we will define in Sec. C.5 below. Then the solution functions are modified such that s_i only depends on the ancestors e_{anc_i} according to the inferred topological order:

$$s_i(e_i; e_{\setminus i}) \rightarrow s_i(e_i; e_{\text{anc}_i}). \quad (19)$$

This is implemented with a suitable masking layer in the neural network implementation of s_i . We find that this form of inductive bias in the prior helps with learning cleanly disentangled representations.

Second, we fix the intervention encoders to the deterministic,

$$q^{\text{deterministic}}(I|x, \tilde{x}) = \begin{cases} 1 & I = \arg \max_I q(I|x, \tilde{x}) \\ 0 & \text{else,} \end{cases}$$

$$q(e, \tilde{e}, I|x, \tilde{x}) = q^{\text{deterministic}}(I|x, \tilde{x})q(e, \tilde{e}|x, \tilde{x}, I). \quad (20)$$

This further improves the training efficiency.

We summarize the whole ILCM training procedure in Alg. 1. The separation of phase 2 and 3—first training the encoder with a simplified prior, then training the solution functions—improved the success of our method substantially. Adding the pre-training and fine-tuning phases 1 and 4 slightly improved the efficiency of the training, but is not critical.

We use the Adam optimizer [39] with a cosine annealing schedule [40], which is restarted at the beginning of training phases 3 and 4. The hyperparameters differ slightly between experiments and will be given in Sec. D.

C.4 Identifiability

We will now show that our identifiability result extends to implicit latent causal models. We construct an equivalence $\Omega : \text{ILCM} \rightarrow \text{ELCM}$ between ILCMs and ELCMs, which preserves the weakly supervised distribution $p(x, \tilde{x})$. This gives an equivalence relation on ILCMs, namely if their corresponding ELCMs are isomorphic according to Def. 9. A direct corollary of Thm. 1 is then that the weakly supervised distributions of ILCMs $\mathcal{N}, \mathcal{N}'$ are equal, $p_{\mathcal{N}}(x, \tilde{x}) = p_{\mathcal{N}'}(x, \tilde{x})$, if and only if they are equivalent, $\mathcal{N} \sim \mathcal{N}'$.

To construct the map Ω between an ILCM \mathcal{N} and ELCM \mathcal{M} , let both have equal: solution function $s : \mathcal{E} \rightarrow \mathcal{Z}$, noise distribution $p(\epsilon)$, intervention distribution $p(I)$, intervention encoder. Let the encoder $q(e|x)$ of \mathcal{N} be equal to the encoder $q(z|x)$ of \mathcal{M} , post-composed with the inverse solution function $s^{-1} : \mathcal{Z} \rightarrow \mathcal{E}$, and the decoder be pre-composed with the solution function. Let the explicit graph in \mathcal{M} equal the graph induced by the solution function of \mathcal{N} , with $\forall i \neq j$, the edge $i \rightarrow j$ exists if $\exists \epsilon$ such that $\partial s(\epsilon)_j / \partial \epsilon_i \neq 0$.

To map from an ILCM \mathcal{N} to an ELCM \mathcal{M} , we pick the intervened causal mechanism \tilde{f}_i as any map such that the causal distribution $p(\tilde{z}_i) = (\tilde{f}_i)_* p(e_i)$ of \mathcal{M} equals the post-intervention causal-variable prior $\tilde{\pi}(\tilde{z}_i)$ in \mathcal{N} . For \mathbb{R} -valued variables and fully supported distributions with smooth densities, there are exactly two possible choices for \tilde{f}_i . To map from an ELCM \mathcal{M} to an ILCM \mathcal{N} , we set $\tilde{\pi}(\tilde{z}_i) := (\tilde{f}_i)_* p(e_i)$.

Following the definitions of the weakly supervised distributions, it is easy to see that Ω preserves weakly supervised distribution, so that if $\mathcal{M} = \Omega(\mathcal{N})$, then $p_{\mathcal{M}}(x, \tilde{x}) = p_{\mathcal{N}}(x, \tilde{x})$, and if $\mathcal{N} = \Omega^{-1}(\mathcal{M})$, then $p_{\mathcal{M}}(x, \tilde{x}) = p_{\mathcal{N}}(x, \tilde{x})$. This proves that our identifiability result of ELCMs also applies to ILCMs.

C.5 Graph inference

ILCMs do not contain an explicit graph representation, but the causal structure is implicitly represented by the learned solution functions. We propose two algorithms for causal discovery based on a

trained ILCM model.

ILCM-E We can perform causal discovery in a two-stage procedure. After training an ILCM to learn the causal representations, we use an off-the-shelf method for causal discovery on the learned representations. Since the ILCM allows us to infer intervention targets, we can use intervention-based algorithms. In this paper, we use ENCO [28], a recent differentiable causal discovery method that exploits interventions to obtain acyclic graphs without requiring constrained optimization. Alternatives to ENCO include DCDI [27] and GIES [30].

ILCM-H Alternatively, we can unearth the causal structure encoded in the learned solution functions s_i , which map noise variables to causal variables. We introduce a heuristic algorithm that can find the causal graph \mathcal{G} and the causal mechanisms f_i from a trained ILCM. It proceeds in three steps:

1. *Computing the topological order:* To determine the topological order of the causal graph, we use the property that after convergence, the solution function $z_i = s_i(e_i; e)$ will only depend on the ancestors of e_i . This allows us to define a heuristic that determines whether z_i is an ancestor of z_j . For each pair (i, j) , we compute

$$\text{ancestry}(i, j) = d\left(s_j(e_j; e), s_j(e_j; \text{mask}_i[e])\right). \quad (21)$$

Here $d(\cdot, \cdot)$ is a distance measure between two functions; in practice, we use the expected MSE over a validation dataset. The function $\text{mask}_i[e]$ replaces the i -th component of e with uninformative input, for instance median of that component computed over the training dataset.

After computing these ancestry scores, we can compute a topological order by sorting the variables such that likely ancestors appear before their likely descendants according to this heuristic. We do this with a greedy algorithm.

2. *Extracting the causal mechanisms:* Next, we compute the causal mechanisms f_i such that $z_i = f_i(e_i; z_{\text{anc}_i})$. We begin by setting i to the root node (the first variable in the topological order computed in step 1) and proceed in topological order. At every step we set

$$f_i(e_i; z_{\text{anc}_i}) = s_i(e_i; \hat{e}) \quad \text{with} \quad \hat{e}_j = \begin{cases} f_j^{-1}(z_j; z_{\text{anc}_j}) & j \in \text{anc}_i \\ \text{mask}[e_j] & \text{otherwise.} \end{cases} \quad (22)$$

3. *Finding causal parents:* Finally, we check whether an ancestor z_i is a parent of a node z_j by testing whether f_j explicitly depends on z_i . Again, we use a heuristic measure of functional dependence:

$$\text{paternity}(i, j) = d\left(f_j(e_j; z_{\text{anc}_j}), f_j(e_j; \text{mask}_i[z_{\text{anc}_j}])\right). \quad (23)$$

We then construct the causal graph by thresholding on this heuristic. This gives us the inferred adjacency matrix

$$\hat{A}_{ij} = \begin{cases} 1 & i \in \text{anc}_j \quad \text{and} \quad \text{paternity}(i, j) > p_{\min} \\ 0 & \text{else} \end{cases} \quad (24)$$

where $p_{\min} > 0$ is a hyperparameter.

The heuristic algorithm (ILCM-H) does not require any optimization and is thus computationally more efficient, but arguably less principled than the likelihood-based ENCO approach (ILCM-E). In our experiments, the ILCM-H approach finds the correct graph in 7 out of the 8 datasets, while ILCM-E always yields the correct causal graph.

D Experiments

D.1 General setup

Baselines We compare our ILCM-E and ILCM-H results (which differ only by the graph inference algorithm, as described above) to three baseline methods. The *disentanglement VAE* (dVAE) method is a VAE for paired data with individual latent components changing between the pre-intervention

latents and the post-intervention latents, but without causal structure. We implement it by using an ILCM, but enforce a trivial causal graph by not allowing the solution functions $s_i(\cdot; e)$ to depend on e .

Our second baseline is an unstructured β -VAE, which treats pre-intervention and post-intervention data as i. i. d. and models both with a standard Gaussian prior.

Finally, we include a slot attention baseline. We use as many slots as there are latents. We break the symmetry between the slots by initialising the slots not with a random vector, but with a different learned vector per slot, as is done in Ref. [41]. We choose a six-dimensional latent for each slot.

Metrics We evaluate the disentanglement of the learned causal variables by computing the DCI disentanglement, completeness, and informativeness scores [32]. They are based on a feature importance matrix that quantifies how important each model latent is for predicting each ground-truth causal factor; we compute the feature importance matrix with gradient boosted trees in scikit-learn’s implementation with default parameters [42]. There are many other disentanglement metrics, but empirically these tend to be highly correlated with the DCI disentanglement score [3], so we omit them here for simplicity. For the slot attention models, we add up the contribution of the latent dimensions of each slot, to get a importance matrix between slots and ground truth causal variables.

The quality of intervention inference is evaluated with the accuracy of the intervention encoder. Since we can only identify causal variables and intervention targets up to a permutation, we compute this accuracy for any possible permutation of the causal variables and then report the best result.

Finally, we evaluate the quality of the inferred causal graphs. We identify the ground-truth variables with the corresponding learned causal variables based on the importance matrix computed for the DCI disentanglement score [32]. We then compute the structural Hamming distance (or graph edit distance) between the learned graph and the true graph. As an example, consider the case of two causal variables, where the ground-truth graph is $z_1 \rightarrow z_2$, the ILCM graph is $z'_1 \rightarrow z'_2$, and the ground-truth and learned variables are mapped to each other as $z_1 \leftrightarrow z'_2$ and $z_2 \leftrightarrow z'_1$. Then the structural Hamming distance will be 1, as the cause and effect are flipped in the learned model.

D.2 2D toy experiment

Dataset We first demonstrate LCMs in a pedagogical toy experiment with $\mathcal{X} = \mathcal{Z} = \mathbb{R}^2$. Training data is generated from a nonlinear SCM with the graph $z_1 \rightarrow z_2$ and mapped to the data space through a randomly initialized normalizing flow.

In particular, we have that $z_1 \sim \mathcal{N}(z_1; 0, 1^2)$ and $z_2 \sim \mathcal{N}(z_2; 0.3z_1^2 + 0.6z_1, 0.8^2)$. This latent data is mapped to the data space $\mathcal{X} = \mathbb{R}^2$ with a randomly initialized coupling flow with five affine coupling layers interspersed with random permutations of the dimensions. For the weakly supervised setting we use a uniform intervention prior over $\{\emptyset, \{z_1\}, \{z_2\}\}$. We generate 10^5 training samples, 10^4 validation samples, and 10^4 evaluation samples (where each sample is one pair (x, \tilde{x}) of pre- and post-intervention data).

Architecture The noise encoder and noise decoder are Gaussian, with mean and standard deviation computed by fully connected networks. The solution functions are implemented as affine transformations with slope and offset computed as a function of the pre-intervention noise encodings, also implemented with fully connected networks. For each MLP, we use two hidden layers with 100 units each and ReLU activations.

Training Models are trained using the procedure described in Sec. C.3. We train for $9 \cdot 10^4$ steps using a batch size of 100 and an initial learning rate of 10^{-3} . The weights of the different loss terms and regularizers are as follows: β is initially set to 0 and increased to its final value of 1 during training, $\alpha = 10^{-2}$, and $\gamma = 0$ throughout training. For each method, we train models with three random seeds and in the end select the median run according to the validation loss.

D.3 Causal3DIdent experiments

Dataset In the Causal3DIdent experiments we consider six different datasets, each generated from a different causal graph, SCM, and decoder. The six causal graphs we consider are:

- the trivial graph $\circ \circ \circ$,

Table 2: Detailed experiment results. We compare our ILCM-E (using ENCO for graph inference) and ILCM-H (with a heuristic for graph inference) to disentanglement VAE (dVAE-E), unstructured β -VAE, and slot attention baselines. We show the DCI scores (disentanglement D , completeness C , informativeness I), the accuracy of intervention inference, the learned graph, and the structural Hamming distance (SHD) between learned and true graph. Best results in bold.

Dataset	True graph	Method	D	C	I	Int. accuracy	Learned graph	SHD
2D toy data		ILCM-E (ours)	0.99	0.99	0.00	0.96		0
		ILCM-H (ours)	0.99	0.99	0.00	0.96		0
		dVAE	0.35	0.50	0.01	0.96		1
		β -VAE	0.52	0.53	0.00	–	n/a	–
Causal3DIdent		ILCM-E (ours)	0.99	0.99	0.00	0.98		0
		ILCM-H (ours)	0.99	0.99	0.00	0.98		0
		dVAE	1.00	1.00	0.00	0.98		0
		β -VAE	0.94	0.94	0.00	–	n/a	–
		Slot attention	0.90	0.90	0.01	–	n/a	–
		ILCM-E (ours)	1.00	1.00	0.00	0.98		0
	ILCM-H (ours)	1.00	1.00	0.00	0.98		0	
	dVAE	0.91	0.91	0.00	0.98		1	
	β -VAE	0.92	0.92	0.00	–	n/a	–	
	Slot attention	0.56	0.84	0.02	–	n/a	–	
		ILCM-E (ours)	0.99	0.99	0.00	0.98		0
		ILCM-H (ours)	0.99	0.99	0.00	0.98		0
		dVAE	0.83	0.83	0.00	0.98		2
		β -VAE	0.63	0.71	0.00	–	n/a	–
		Slot attention	0.42	0.59	0.02	–	n/a	–
		ILCM-E (ours)	0.99	0.99	0.00	0.98		0
	ILCM-H (ours)	0.99	0.99	0.00	0.98		0	
	dVAE	0.79	0.81	0.00	0.98		2	
	β -VAE	0.63	0.68	0.01	–	n/a	–	
	Slot attention	0.87	0.87	0.03	–	n/a	–	
		ILCM-E (ours)	0.99	0.99	0.00	0.98		0
		ILCM-H (ours)	0.99	0.99	0.00	0.98		0
		dVAE	0.80	0.81	0.01	0.98		2
		β -VAE	0.28	0.52	0.16	–	n/a	–
Slot attention		0.32	0.35	0.04	–	n/a	–	
ILCM-E (ours)		0.99	0.99	0.00	0.98		0	
ILCM-H (ours)	0.99	0.99	0.00	0.98		0		
dVAE	0.60	0.64	0.00	0.98		3		
β -VAE	0.57	0.61	0.01	–	n/a	–		
Slot attention	0.53	0.67	0.01	–	n/a	–		
CausalCircuit		ILCM-E (ours)	0.97	0.97	0.00	1.00		0
		ILCM-H (ours)	0.97	0.97	0.00	1.00		0
		dVAE-E	0.34	0.55	0.00	1.00		5
		β -VAE	0.39	0.43	0.00	–	n/a	–
		Slot attention	0.39	0.82	0.00	–	n/a	–



Figure 10: Effect of varying the learned causal factors on the image in the Causal3DIdent dataset. We encode a single test images (middle column) into the three learned causal variables. We then vary each of these causal factors in isolation (without performing interventions, that is, without including the causal effects on other variables) and show the reconstructed images. The ILCM (top) learns a representation that is quite disentangled: z_1 largely corresponds to the spotlight color, z_2 to the spotlight position, and z_3 to the object color. In contrast, the acausal dVAE baseline entangles the object color and spotlight color in its learned representation z_1 .

- single edge
- the chain
- the fork
- the collider
- the full graph

For each of these subsets, we randomly generate a nonlinear SCM with heteroskedastic noise: for each causal mechanism, we randomly initialize an MLP that outputs the scale and shift of an affine transformation as a function of the causal parents. We choose an MLP initialization scheme that emphasizes nontrivial, nonlinear causal effects. We then identify a random permutation of the three causal variables with three high-level concepts in the Causal3DIdent dataset: the object hue, the spotlight hue, and the spotlight position. We use the following causal graphs:

- single edge: object hue \rightarrow spotlight position;
- chain: spotlight position \rightarrow spotlight hue \rightarrow object hue;
- fork: spotlight hue \rightarrow spotlight position, object hue;
- collider: spotlight hue \rightarrow object hue \leftarrow spotlight position;

- full graph: spotlight hue \rightarrow object hue \rightarrow spotlight position, spotlight hue \rightarrow spotlight position.

Since all of these properties are defined on a range $[0, 2\pi)$, we apply an elementwise arctanh transform and rescaling to our variables such that they populate a subset of $[0, 2\pi)$. This also avoids topological issues. Next, we generate images in 64×64 resolution following the procedure described in Ref. [14]. We use Blender [43] to generate 3D rendered images based on the previously defined causal variables. To increase diversity of the six datasets, we render each dataset with a different object: Teapot [44], Armadillo [45], Hare [46], Cow [47], Dragon [48], and Horse [49]. We generate 10^5 training samples, 10^4 validation samples, and 10^4 evaluation samples.

Architecture For the noise encoder and noise decoder we use a convolutional architecture with four residual blocks, using downsampling via average-pooling and bilinear upsampling, respectively. We do not use BatchNorm, as we found that that can lead to practical issues when images in a batch are very similar. The output of the convolutional layers is then fed through a fully connected network with two hidden layers, 64 units each, and ReLU activations. For each of the three latents output by the encoder, we apply an additional elementwise MLP with one hidden layers, 16 units each, and ReLU activations. For the solution functions we use the same architecture as in the 2D toy data.

Training Models are trained using the procedure described in Sec. C.3. We train for $2.5 \cdot 10^5$ steps using a batch size of 64 and an initial learning rate of $8 \cdot 10^{-5}$. The weights of the different loss terms and regularizers are as follows: β is initially set to 0 and increased to its final value of 0.05 during training, $\alpha = 10^{-2}$, and $\gamma = 5$ throughout training. For each method, we train models with three random seeds and in the end select the median run according to the validation loss.

Results In the main paper, we report aggregate metrics averaged over the subsets in Tbl. 1 and demonstrate intervention inference in Fig. 5. In the latter, we infer intervention targets the intervention encoder $q(I|x, \tilde{x})$, find the pre- and post-intervention noise encodings with the noise encoder, $e, \tilde{e} \sim q(e, \tilde{e}|x, \tilde{x}, I)$, intervene in the latent space by constructing a new noise encoding consisting of $e_{\setminus I}$ and \tilde{e}_I , and push to the data space with the decoder.

In addition to the results shown in the main paper, we show metrics for each separate subset in in Tbl. 2 and visualize the disentanglement properties of the learned representations in Fig. 10.

D.4 CausalCircuit experiments

Dataset We introduce the new CausalCircuit dataset. This environment is built in the MuJoCo simulator [33], using a model of the TriFinger robotic platform [50], of which we use a single finger. There are four causal variables: the three lights and the robot arm. The arm state is the position along an arc that goes over three buttons. The position on the arc is translated into actuator angles using an inverse kinematic model. To obtain a sample, the arm is moved away from the buttons, then lowered to the desired position, after which a rendering is recorded. Each red, green and blue button then has a pressed state b_R, b_G, b_B that depends on how far the button is touched from the center and scales linearly in the radial distance from 0 to 1. The causal model for the red, green and blue light variables and the arm z_A then is:

$$\begin{aligned}
 v_R &= 0.2 + 0.6 * \text{clip}(z_G + z_B + b_R, 0, 1) \\
 v_G &= 0.2 + 0.6 * b_G \\
 v_B &= 0.2 + 0.6 * b_B \\
 z_R &\sim \text{Beta}(5v_R, 5 * (1 - v_R)) \\
 z_G &\sim \text{Beta}(5v_G, 5 * (1 - v_G)) \\
 z_B &\sim \text{Beta}(5v_B, 5 * (1 - v_B)) \\
 z_A &\sim \text{Uniform}(0, 1)
 \end{aligned}$$

The scene is rendered in 512×512 pixels using the MuJoCO renderer.

Dimensionality reduction Rather than training directly on images, we found it beneficial for fast experimentation to first condense the image datasets into a lower-dimensional representation and

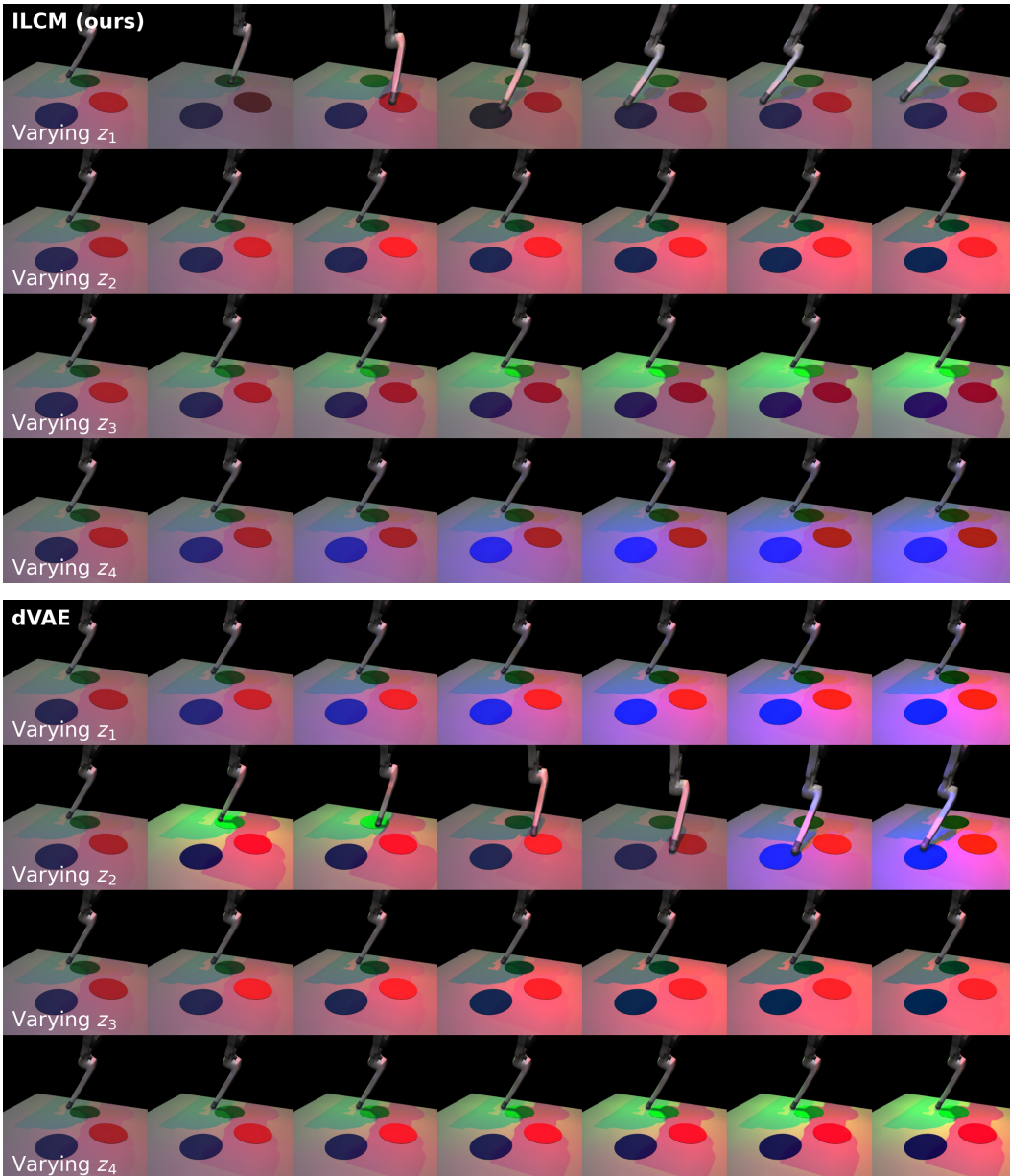


Figure 11: Effect of varying the learned causal factors on the image in the CausalCircuit dataset. We encode a single test images (left column) into the four learned causal variables. We then vary each of these causal factors in isolation (without performing interventions, that is, without including the causal effects on other variables) and show the reconstructed images. The ILCM (top) learns a representation that is quite disentangled: z_1 corresponds to the blue light, z_2 to the green light, z_3 to the robot arm position, and z_4 to the red light. In contrast, the acausal dVAE baseline entangles the different lights and the robot arm position in its learned latent factors.

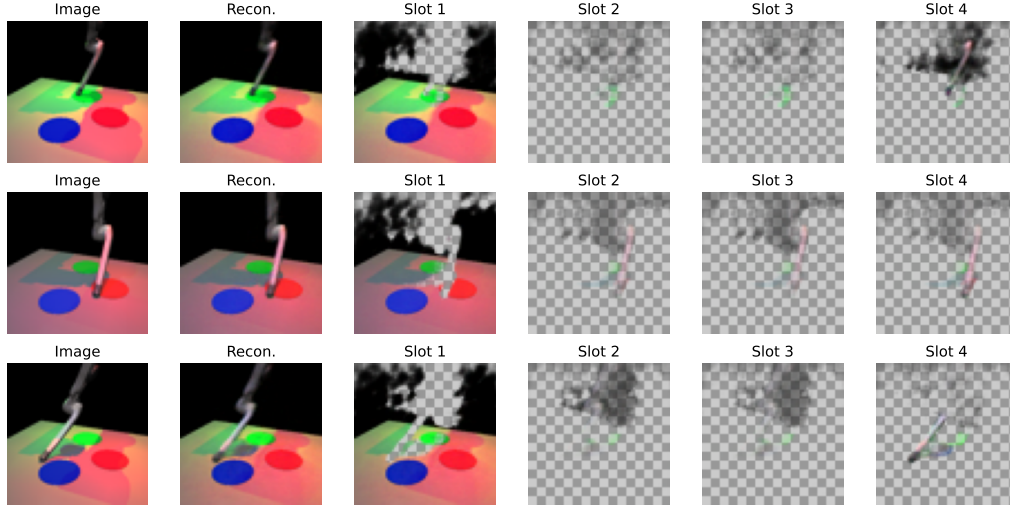


Figure 12: The slots found by slot attention. We see that the slots do not correspond to the causal variables. Only the arm is disentangled from the buttons and lights.

then train both ILCMs and baselines excluding slot attention) on that data. We used a β -VAE with a standard Gaussian prior with 16 latent dimensions; the encoder and decoder follow the same architecture as for the Causal3DIdent dataset. This VAE was trained for $8.5 \cdot 10^4$ steps using the Adam optimizer, an initial learning rate of $3 \cdot 10^{-4}$, cosine annealing, and batchsize 128.

For slot attention, we reduced the resolution to 64×64 , as we found it difficult to train the model on the full resolution 512×512 .

Architecture On this dimensionality-reduced, 16-dimensional data, we use fully connected networks for noise encoder and noise decoder, each with five hidden layers with 64 units each and ReLU activations. The solution functions have the same architecture as in the other experiments.

Training Models are trained using the procedure described in Sec. C.3. We train for $9.4 \cdot 10^4$ steps using a batch size of 64 and an initial learning rate of $3 \cdot 10^{-4}$. The weights of the different loss terms and regularizers are as follows: β is initially set to 0 and increased to its final value of $3 \cdot 10^{-4}$ during training, $\alpha = 10^{-2}$, and $\gamma = 10$ throughout training. For each method, we train models with three random seeds and in the end select the median run according to the validation loss.

Results In addition to the results in the main paper, Fig. 11 shows that our ILCM model successfully disentangled the causal factors, while the dVAE baseline failed at that task. Similarly, in Fig. 12 we see that the slot attention model fails to assign the causal variables into separate slots. We presume this is because the lights blend into each other, making them only describable by a single slot.

D.5 Graph scaling

Dataset Finally, we study the scaling of LCMs with the size of the causal graph. We generate synthetic datasets with $n \in \{2, 4, 6, 8, 10, 12, 15, 20\}$ causal variables. For each dimensionality, we generate three different datasets with different SCMs and maps to the data space. The causal graphs are generated by fixing a topological order, then for each edge consistent with the topological order we draw a Bernoulli random variable with probability $\frac{1}{2}$ to determine whether the edge exists. The SCMs are additive noise models with linear causal effects, $z_j = \epsilon_j + \sum_{j \in \text{pa}_i} a_{ij} z_i$, where $\epsilon_j \sim \mathcal{N}(0, 1)$ and the coefficients a_{ij} are drawn from a Gaussian mixture model with two equally likely components with means ± 1 and standard deviation 0.3. (Drawing the strengths of the causal effects from such a mixture model makes it unlikely to draw a causal effect very close to 0, which corresponds to a faithfulness violation.) Causal variables are mapped to the data space \mathbb{R}^n by a randomly sampled $SO(n)$ transformation.

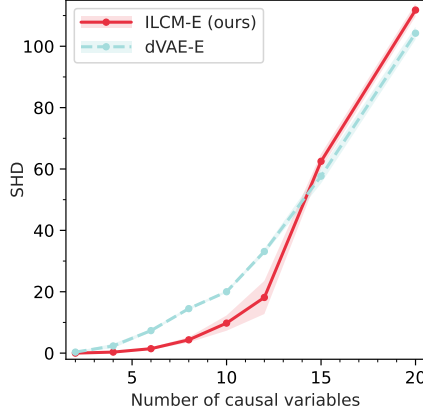


Figure 13: Scaling with graph size. We show the mean SHD between the learned and true causal graph (lower is better) and the standard error of the mean. The graphs found with ILCM-E are of a high quality for up to around 10 causal variables, but ILCM does not yet scale to even larger systems.

Architecture We use fully connected networks for noise encoder and noise decoder, each with two hidden layers with 64 units each and ReLU activations. The solution functions have the same architecture as in the other experiments.

Training Models are trained using the procedure described in Sec. C.3. We train for $1.4 \cdot 10^5$ steps using a batch size of 64 and an initial learning rate of $3 \cdot 10^{-4}$. The weights of the different loss terms and regularizers are as follows: β is initially set to 0 and increased to its final value of 1 during training, $\alpha = 10^{-2}$, and $\gamma = 1$ throughout training. We find it beneficial to not fix the topological order during training. For each dataset and each method, we train models with three random seeds; in the end we take the mean over all datasets and seeds.

Results In addition to the results in the main paper, Fig. 13 shows the accuracy of the learned causal graphs as a function of the size of the system inferred with ENCO. For up to around 10 causal variables, our method lets us disentangle the causal variables reliably, and the graphs found by ILCM are more accurate than those found by the baseline. Scaling ILCMs to even larger system will require additional research.

E Explicit latent causal models

E.1 Setup

Explicit latent causal models (ELCMs) are variational autoencoders, in which the latent variables are the causal variables of an SCM. They consist of a causal encoder $q(z|x)$, decoder $p(x|z)$, and a prior $p(z, \tilde{z})$ that encodes the causal structure.

Intervention targets can either be inferred with an intervention encoder $q(I|x, \tilde{x})$, similar to our ILCM model, or be marginalized over explicitly as $p(z, \tilde{z}) = \sum_I p(I)p(z, \tilde{z}|I)$. We have experimented with both settings, for concreteness we here focus on the second, simpler setup.

The conditional prior $p(z, \tilde{z}|I)$ is the weakly supervised distribution of an SCM. They are parameterized through the causal graph \mathcal{G} , neural causal mechanisms $f_i(\epsilon_i; z_{\text{pa}_i})$, and noise base distributions. To learn the graph, the simplest option is to instantiate one LCM per graph equivalence class, train them, and select the model with the lowest validation loss. Alternatively, we can parameterize the graph in a differentiable way [26–29] and learn the graph together with the other components through gradient descent.

We contrast the VAE setup of ILCMs and ELCMs in Tbl. 3.

Like ILCMs, ELCMs are trained on a VAE loss corresponding to a variational bound on $\log p(x, \tilde{x})$. Following common practice in causal discovery [27, 28, 51], we incentivize learning the sparsest

Table 3: Differences between explicit and implicit latent causal models (ELCMs and ILCMs). Optional learnable components are shown in parantheses.

¹For simplicity, in this section we describe an ELCM implementation without intervention encoder. ²We achieved the best results when inferring and enforcing a topological order only for the last phase of ELCM training, see Sec. C.3.

	Explicit latent causal model	Implicit latent causal model
Latent variables	causal variables (z, \tilde{z}) intervention targets I	noise encodings (e, \tilde{e}) intervention targets I
Learnable components	encoder $q(z x)$ decoder $p(x z)$ (intervention encoder $q(I x, \tilde{x})$) ¹ graph \mathcal{G} causal mechanisms $f_i(\epsilon_i; z_{\text{pa}_i})$	encoder $q(e x)$ decoder $p(x e)$ (intervention encoder $q(I x, \tilde{x})$) (topological order) ² solution functions $s_i(e_i; e_{\setminus i})$

graph compatible with the data distribution by adding a regularization term proportional to the number of edges in the graph to the loss.

E.2 Experiments



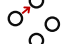
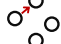
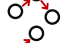
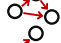
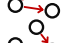
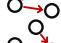


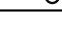
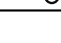
Dataset We experiment with ELCMs in similar datasets as we did in the main paper with ILCMs. In particular, we report results on six Causal3DIdent variations. However, we performed these datasets on an earlier iteration of these datasets: while main parameters of the scenes and the causal graphs are the same as in the experiments reported in the main paper, the ground-truth causal mechanisms are different. The metrics reported here are therefore not directly comparable to the ILCM results in the main paper.

Hyperparameters Our ELCM architecture and training follows similar hyperparameters to our ILCM experiments. We experimented with various graph parameterizations and sampling procedures, including directed edge existence probabilities with Gumbel-Softmax sampling [26, 27], undirected edge existence probabilities and edge orientation probabilities [28], and the parameterization through edge existence probabilities and a distribution over permutations [29]. While our implementation all of these methods were able to successfully learn causal graphs given the true causal variables, we were not able to reliably learn the representations and the graph jointly. We observed a higher success rate when training separate models for different fixed DAGs and then selecting the best graph based on the validation loss. The results reported below were generated with this exhaustive graph search strategy. Again we show the median run out of three random seeds according to the validation loss.

Results In Tbl. 4 we show disentanglement scores and learned graphs. The results are mixed: in some of the datasets the graph was correctly identified and the variables are disentangled, while in others the model failed at both tasks. Notably, we find that the results strongly vary with the initialization (i. e. the random seed). In Tbl. 4 we only show the median result out of three runs, but in almost all datasets there is one random seed that lead to successful disentanglement (always with the best training and validation loss) and one random seed that led to failed disentanglement (with a worse training and validation loss). ELCM training is thus much less robust than our ILCM experiments, where the results were largely stable across random seeds.

Discussion This result hints at the presence of local minima in the loss landscape that models can get stuck in when starting from an unlucky initialization. By manually analyzing the trained ELCMs, we find that one common failure mode is that models learn variables that are to some extent disentangled and the graph has the right skeleton, but some of the causal effects are wrongly oriented (swapping cause and effect). Such graphs are often in the same Markov equivalence class as the correct graph, which is why such a model can minimize the observational contribution $-\log p(z)$ to the overall loss. Smoothly changing the representations would take the model out of the Markov equivalence class, increase this term and thus the overall loss; this configuration thus presents a local loss minimum. The same phenomenon occurs in our experiments with differentiable graph parameterizations.

Table 4: ELCM experiments on Causal3DIdent datasets. We show the learned causal graph, the structural Hamming distance SHD between the learned and the true graph and the DCI disentanglement score (D). The datasets differ slightly from the ones used in our main experiments, so metrics are not directly comparable.

True graph	D	Learned graph	SHD
	1.00		0
	0.99		0
	0.45		3
	0.98		0
	0.98		0
	0.43		2

F Potential societal impact

Although we expect the immediate societal impact of this work to be negligible, more generally causal representation learning may have significant impact in the longer run. It will allow for the discovery of potential causal relationships in unstructured human-centric data. This may be beneficial, for example as it allows one to inspect if a model has learned sensible or fair causal relationships. A potential risk is that, for example because certain confounding variables are not discovered from the data, the algorithm may conclude erroneously that sensitive variables are causes of relevant outcomes. Users of the algorithms should be cautious of that.